

Luciano de Oliveira Júnior

Coastal counter-currents setup patterns in the Gulf  
of Cadiz: an indication of their forcing factors



**UNIVERSIDADE DO ALGARVE**  
**FACULDADE DE CIÊNCIAS E TECNOLOGIA**

**2017**

Luciano de Oliveira Júnior

# Coastal counter-currents setup patterns in the Gulf of Cadiz: an indication of their forcing factors

Master in Marine and Coastal Sciences

Work performed under the supervision of:

Erwan Garel

Paulo Relvas



**UNIVERSIDADE DO ALGARVE**  
**FACULDADE DE CIÊNCIAS E TECNOLOGIA**

**2017**

# Coastal counter-currents setup patterns in the Gulf of Cadiz: an indication of their forcing factors

## Declaração de autoria de trabalho

Declaro ser o(a) autor(a) deste trabalho, que é original e inédito. Autores e trabalhos consultados estão devidamente citados no texto e constam da listagem de referências incluída

A handwritten signature in black ink, reading "Luciano de Oliveira Júnior". The signature is written in a cursive style with large, flowing letters.

Luciano de Oliveira Júnior

## **Copyright**

A Universidade do Algarve reserva para si o direito, em conformidade com o disposto no Código do Direito de Autor e dos Direitos Conexos, de arquivar, reproduzir e publicar a obra, independentemente do meio utilizado, bem como de a divulgar através de repositórios científicos e de admitir a sua cópia e distribuição para fins meramente educacionais ou de investigação e não comerciais, conquanto seja dado o devido crédito ao autor e editor respetivos.

## **Acknowledgments**

My most sincere thanks go to Erwan Garel, my supervisor who had always his office door open for me and patiently clarified my doubts. I thank him to leaving me free to follow my intuitions and also to lead me in the right directions when needed.

I also thank professor Paulo Relvas for giving me the chance to make part of a subject where he is an international reference.

Especially, I thank Tainá Garcia da Fonseca, who patiently revised my texts and advised me on the scientific writing. She always motivated me and gave me support in the most difficult moments.

I would also like to acknowledge IPMA for being one of the originators of the data set used for this work and a special thanks to Teresa Drago who has been putting a lot of effort to maintain the data acquisition active.

## Resumo

As contra-correntes costeiras (CCCs) ao longo da costa são características frequentes dos sistemas de afloramento costeiro, onde alternam temporariamente com jatos de direção oposta. Sua ocorrência já foi registada e estudada em diversas regiões do planeta, tais como na costa Sul-Africana, na costa Peruana e na costa oeste norte americana onde o seu estudo tem se desenvolvido com um maior dedicação.

Ao longo da margem norte da plataforma do Golfo de Cádiz, estas CCCs desenvolvem-se de Leste para Oeste numa estreita faixa de largura que pode chegar até 30 km. As CCCs são responsáveis por elevar rapidamente a temperatura durante os períodos de afloramento no verão e durante o inverno o oposto acontece, uma vez que a afluência de águas provenientes do interior do continente torna-se mais frequente na região. Apesar de não representarem uma característica permanente da região, sua ocorrência acontece em média uma vez por semana com duração de 3 dias.

Na região do Golfo de Cádiz, acredita-se que as CCCs possam apresentar um potencial declínio na qualidade da água. Estas correntes podem ser responsáveis pelo transporte de águas pobres em nutrientes ou o transporte de poluentes. No campo da biologia marinha, seu estudo é também de grande interesse, uma vez que a dispersão de larvas pode estar associada a estas correntes. O conhecimento mais aprofundado da circulação nesta região irá também influenciar na construção de modelos de previsão mais precisos. No entanto, o processo de desenvolvimento e as forças motrizes responsáveis continuam por se descrever e comprovar.

Actualmente existem várias teorias para o seu desenvolvimento. A primeira teoria explica o desenvolvimento das CCCs baseando-se na existência de uma inclinação da superfície do mar ao longo da costa. Esta diferença de nível geraria um gradiente horizontal de pressão e essa seria a força principal para iniciar o fluxo. Fenómenos típicos de verão como o afloramento costeiro ou o aquecimento das águas pouco profundas da região mais oriental do Golfo poderiam ser os responsáveis por gerar tal desnível da superfície do mar. Outra teoria relaciona as CCCs com a influência da circulação do mar aberto e explica que, águas Atlânticas ao entrarem no Golfo de Cádiz interagem com águas provenientes do mar Mediterrâneo e são forçadas a recircular ciclonicamente. Finalmente a influência de ventos favoráveis que podem ocorrer em qualquer parte do ano, porém com maior frequência nos períodos de outono e inverno. Eventos de CCCs sem a presença destes mesmos ventos podem acontecer, o que exclui os mesmos como o principal agente, porém sua influência não deve ser ignorada uma vez que estes ventos ocorrem com alguma frequência e força suficiente para influenciar na circulação da região.

As actuais teorias apresentadas anteriormente implicam sazonalidade na ocorrência dos agentes forçadores das CCCs, porém um estudo recente mostrou que estas correntes podem acontecer em qualquer período do ano sem grande diferença de frequência entre inverno e verão. Tendo isto em conta surgiu então as questões que motivaram este trabalho: será que as CCCs são causadas sempre pelos mesmos factores? Se existirem mais do que uma força envolvida será que o fluxo desenvolver-se-á de forma distinta. Para tentar responder a esta questão este trabalho foi elaborado com o objectivo de analisar o desenvolvimento CCCs focando no momento de inversão (isto é, o momento de mudança de sentido de Leste para Oeste). Na presença de diferentes forças actuantes foi esperado diferentes tipos de perfis verticais do fluxo e uma categorização foi efectuada juntamente com uma indicação das possíveis forças responsáveis.

Este estudo baseia-se em séries temporais de velocidade plurianuais (2008-2017), obtidas através de ADCP, e registadas em uma mesma localização a 23 m de profundidade durante 13 campanhas de até 3 meses de duração cada uma. A análise centra-se nos perfis de velocidades de componente longitudinal durante inversões. Um conjunto de parâmetros foi derivado da estrutura vertical e temporal do fluxo para identificar diferentes tipos de inversões e a hipotetizar possíveis mecanismos que justifiquem o desenvolvimento das CCCs. Para tal foram consideradas 3 camadas do fluxo: Velocidade média da coluna de água, camadas junto ao fundo e camada junto à superfície. Os resultados mostram que em média o processo de inversão apresenta um período de 2 dias em todas as camadas, e que as camadas superiores apresentam sempre uma aceleração mais acentuada durante as inversões. Os resultados mais significantes mostram que 79% das inversões começam junto ao fundo, propagando-se então para as camadas superiores. A camada inferior também muda de direcção antes da camada superficial para a maioria dos eventos (77%). O cisalhamento vertical neste caso é uma ordem de magnitude maior do que na (menos frequente) situação oposta.

Nenhuma variabilidade sazonal é observada nas ocorrências das CCCs. Entretanto, os parâmetros analisados neste estudo sugerem 3 diferentes tipos de inversões que apresentam um grau de sazonalidade. Tipo A acontecendo preferencialmente durante os meses de outono. Este tipo é definido por inversões em que as camadas do fundo sofrem um desaceleramento (ainda na direcção oposta as CCCs) primeiro, mas a mudança de sentido ocorre primeiramente nas camadas superficiais; Tipo B é o tipo que ocorre com maior frequência durante o ano, mas é predominante nos períodos de primavera-verão. É definido por padrões de inversão mais variáveis. Em particular, as camadas superiores e do fundo são muitas vezes desacopladas durante as inversões, indicando o fortalecimento da baroclinicidade. Neste tipo, as camadas do fundo desaceleram e mudam de sentido primeiro; Tipo 0, predominante no inverno onde as inversões são bem definidas (baixa variabilidade), com padrões de superfície e fundo semelhantes, resultando em um forte componente barotrópico.

Os resultados do presente estudo apresentam pela primeira vez um conjunto de parâmetros em que a estrutura vertical do fluxo durante o desenvolvimento das CCCs é descrita. A categorização de eventos de inversão é proposta com base na correlação das características entre os parâmetros criados e vários tipos de inversão são obtidos, sugerindo que as CCCs são conduzidas por diferentes forças que podem agir separadamente ou em conjunto. Uma breve explicação para justificar os tipos de inversões é apresentada explorando os possíveis factores responsáveis, e um posterior complemento para o estudo das CCCs é sugerido.

**Palavras-chave:** Contra corrente costeira; Golfo de Cádiz; Afloramento costeiro; Circulação induzida pelo vento.

## **Abstract**

Alongshore coastal counter-currents (CCCs) are frequent features of Eastern Boundary Upwelling Systems, where they temporally alternate with upwelling driven jets of opposite direction. Along the northern margin of the Gulf of Cadiz inner shelf, these CCCs are oriented poleward (eastward) and are responsible for sharp temperature increases during the upwelling season, along with potential decline in water quality at the coast.

This research is based on a multi-year ADCP velocity time-series (2008-2017), recorded at a single location (23 m water depth) over 13 deployments up to 3 months-long. The analysis focuses on the water column alongshore velocities during current inversions (i.e., the transition from equatorward upwelling jets to poleward CCCs). A set of parameters were derived from the flow structure to identify distinct types of inversions and to hypothesize about their driving mechanisms. Results showed that 77% of the inversions start near the bed, propagating then to the upper layers. The bottom layer also changes direction before the surface layer for most events (71%). The vertical shear in this case is one order of magnitude greater than in the (less frequent) opposite situation.

No seasonal variability was observed in the CCCs occurrences. However, the parameters analysed in this study suggest different types of inversion between winter and summer. In winter, inversions are well defined (low variability), with similar patterns near the surface and bed layers as a result of a strong barotropic component. In summer, the inversion patterns are more variable. In particular, the upper and bed layers are often importantly decoupled during inversions, indicating the strengthening of baroclinicity. A categorization of inversions events is proposed based on the correlation of the characteristics between the developed parameters. Various types of inversion were obtained, suggesting that CCCs are driven by different forcings that may act separately or jointly.

**Keywords:** Coastal counter-currents; Gulf of Cadiz; Coastal upwelling; Wind-driven circulation.

# Summary

|  |     |
|--|-----|
| Acknowledgments .....                                    | I   |
| Resumo.....  | II  |
| Abstract .....   | IV  |
| List of Figures .....                                    | VII |
| List of Tables.....                                      | X   |
| List of Abbreviations.....                               | X   |
| 1. Introduction .....                                    | 1   |
| 1.1 Motivation .....                                     | 1   |
| 1.2 The Gulf of Cadiz.....                               | 1   |
| 1.3 Definition of coastal counter-currents .....         | 3   |
| 1.4 Development of CCCs .....                            | 4   |
| 1.5 Interaction with the open sea circulation.....       | 5   |
| 1.6 Objectives.....                                      | 6   |
| 2. Materials and methods .....                           | 7   |
| 2.1 Data .....   | 7   |
| 2.2 Data processing .....                                | 9   |
| 2.3 Parameters definition.....                           | 11  |
| 2.4 Temporal periods and seasonal definition.....        | 15  |
| 2.5 Statistical and parameters integrative analysis..... | 16  |
| 3. Results .....   | 16  |
| 3.1 Data overview .....                                  | 16  |
| 3.2 Parameters results.....                              | 17  |
| 3.2.1 Peak delay .....                                   | 17  |
| 3.2.1.1 Seasons.....                                     | 18  |
| 3.2.1.2 Bimonthly scale analysis.....                    | 19  |

|         |                                       |    |
|---------|---------------------------------------|----|
| 3.2.1.3 | Summary of main observations .....    | 21 |
| 3.2.2   | Inversion Duration.....               | 21 |
| 3.2.2.1 | Seasons.....                          | 22 |
| 3.2.2.2 | Bimonthly scale analysis.....         | 24 |
| 3.2.2.3 | Summary of main observations .....    | 25 |
| 3.2.3   | Shear at zero-crossing .....          | 25 |
| 3.2.3.1 | Seasons.....                          | 26 |
| 3.2.3.2 | Bimonthly scale analysis.....         | 28 |
| 3.2.3.3 | Summary of main observations .....    | 30 |
| 3.2.4   | Slope at zero-crossing .....          | 31 |
| 3.2.4.1 | Seasons.....                          | 31 |
| 3.2.4.2 | Bimonthly scale analysis.....         | 32 |
| 3.2.4.3 | Summary of main observations .....    | 34 |
| 3.2.5   | Slope Differences .....               | 34 |
| 3.2.5.1 | Seasons.....                          | 35 |
| 3.2.5.2 | Bimonthly time scale analysis .....   | 36 |
| 3.2.5.3 | Summary of main observations .....    | 38 |
| 3.3     | Parameters integrative analysis ..... | 38 |
| 4.      | Discussion .....                      | 42 |
| 4.1     | Seasonal variability .....            | 46 |
| 4.1.1   | Winter.....                           | 46 |
| 4.1.2   | Spring-summer .....                   | 47 |
| 4.1.3   | Autumn.....                           | 48 |
| 5.      | Conclusions .....                     | 49 |
| 6.      | References .....                      | 50 |
| 7.      | Annex .....                           | 53 |

## List of Figures

|  |    |
|--|----|
| Figure 1.1- Area of interest, isobath 25m, 50m, 200m, 1000m and 2000m. Cape São Vincent (CSV) and Cape Santa Maria (CSM), Strait Gibraltar (SG). .....   | 2  |
| Figure 1.2 - Satellite SST adapted form Relvas and Barton (2005). .....  | 3  |
| Figure 2.1 - ADCP location (yellow circle). .....  | 7  |
| Figure 2.2 - Deployments duration, black bars indicating each deployment duration. ....  | 8  |
| Figure 2.3 - ADCP Workhorse 600kHz, TRDI. ....   | 9  |
| Figure 2.4 - Intensity of signal along the water column. ....  | 9  |
| Figure 2.5 - Current velocity. Raw (red) and detide (black) using Butterworth low pass filter 40 h cut-off period. Negative values are poleward. ....  | 10 |
| Figure 2.6 - Example of detide surface, depth average and near bed velocities. ....  | 11 |
| Figure 2.7 - Peak delay scheme. Black triangles indicate peaks (first derivative =0). Near surface (green), Near bed (red). ....   | 12 |
| Figure 2.8 - Inversion duration scheme. Black triangles indicate peaks before and after zero-crossing (yellow star) .....  | 13 |
| Figure 2.9 - Shear at zero-crossing scheme. Zero crossing in the average layer is indicated by the yellow star. Black triangles indicate the velocity values for the Near surface/bed layer where velocities differences are calculated from. .... | 13 |
| Figure 2.10 - – Slope at zero-crossing scheme. Current’s acceleration computed from the velocity variation 1hour before and 1 hour after zero-crossing (yellow star). ....   | 14 |
| Figure 3.1 - Peak Delay (in hours) all data distribution .....   | 17 |
| Figure 3.2 - Peak delay (in hours) seasonal distribution. Mean represented by asterisks and letters indicates groups differences obtained after Kruskal-Wallis test ( $P > 0.05$ ) and Dunn post hoc comparisons. ....                             | 18 |
| Figure 3.3 Percentages of positive peak delay (green), peak delay > 5 hours (black), together with percentage percentages of peak delay < -5 hours (red) for each season. ....   | 19 |
| Figure 3.4 - Bimonthly peak delay (in hours) distribution. Mean represented by asterisks. ...  | 20 |
| Figure 3.5 - Percentages of peak delay > 5 hours(black), together with percentage percentages of peak delay < -5 hours (red) for period of two months. ....  | 21 |
| Figure 3.6 - Inversion duration in hours all data distribution. Near surface left and near bed right. ....   | 22 |

|   |    |
|---|----|
| Figure 3.7 - Inversion duration (in hours) seasonal distribution. Near surface left and near bed right. Mean represented by asterisks .....   | 23 |
| Figure 3.8 - Percentage of Inversion duration > 50 hours for each Season. Near Surface in black and near bed in red.....  | 23 |
| Figure 3.9 - Inversion duration (in hours) bimonthly distribution. Near surface left and near bed right. Mean represented by asterisks .....  | 24 |
| Figure 3.10 - Percentage of Inversion duration > 50 hours for each Season. Near Surface in black and near bed in red.....   | 25 |
| Figure 3.11 - Shear at zero crossing (m/s) all data distribution. ....  | 26 |
| Figure 3.12 - Shear at zero crossing (m/s) seasonal distribution. Mean represented by asterisks and letters indicates groups differences obtained after Kruskal-Wallis test ( $P > 0.05$ ) and Dunn post hoc comparisons. ....  | 27 |
| Figure 3.13 - Percentages of negative shear at inversion (black), together with percentage of shear >0.1 m/s (red) for each season. ....  | 28 |
| Figure 3.14 - Shear at zero crossing (m/s) bimonthly distribution. Mean represented by asterisks and letters indicates groups differences obtained after Kruskal-Wallis test ( $P > 0.05$ ) and Dunn post hoc comparisons.....  | 29 |
| Figure 3.15 - Percentages of negative shear at inversion (black), together with percentage of shear >0.1 m/s (red) for each period of two months. ....  | 30 |
| Figure 3.16 - Slope at zero-crossing all data distribution. Near the surface layer left and near the bed layer right.....   | 31 |
| Figure 3.17 - Slope at zero-crossing ( $m/s^2$ ) seasonal distribution. Near surface left and near bed right. Mean represented by asterisks and letters indicates groups differences obtained after Kruskal-Wallis test ( $P > 0.05$ ) and Dunn post hoc comparisons. ....  | 32 |
| Figure 3.18- Seasonal percentages of High slope at zero-crossing in black and Low slope at zero crossing in red. Near the surface left and near the bed right. ....   | 32 |
| Figure 3.19 - Slope at zero-crossing ( $m/s^2$ ) bimonthly distribution. Near surface left and near bed right. Mean represented by asterisks and letters indicates groups differences obtained after Kruskal-Wallis test ( $P > 0.05$ ) and Dunn post hoc comparisons ..... | 33 |
| Figure 3.20 - Bimonthly percentages of High slope at zero-crossing in black and Low slope at zero crossing in red. Near the surface left and near the bed right. ....   | 33 |
| Figure 3.21- Slope differences ( $m/s^2$ ) all data distribution. ....  | 35 |
| Figure 3.22 - Slope differences ( $m/s^2$ ) seasonal distribution. Mean represented by asterisks. 35  |    |

|   |    |
|---|----|
| Figure 3.23 - Seasonal percentages of positive slope differences in black and high negative slope differences in red. ....  | 36 |
| Figure 3.24 - Slope differences (m/s <sup>2</sup> ) bimonthly distribution.....   | 37 |
| Figure 3.25 - Bimonthly percentages of positive slope differences in black and high negative slope differences in red. ....   | 37 |
| Figure 3.26 - Seasonal Scatter plot of Shear at zero-crossing versus Slope at zero-crossing. Near the surface left and near the bed right. ....   | 38 |
| Figure 3.27 - Shear at zero-crossing versus peak delay all data. Black letters highlight the inversion types proposed here .....  | 39 |
| Figure 3.28 - Scheme for current inversion Type A, where peak delay is positive and shear at zero-crossing is negative .....  | 39 |
| Figure 3.29 - Scheme for current inversion Type B, where peak delay is positive and shear at zero-crossing is positive.....   | 40 |
| Figure 3.30 - Scheme for current inversion Type C, where peak delay is negative and shear at zero-crossing is negative .....  | 40 |
| Figure 3.31 - Scheme for current inversion Type D, where peak delay is negative and shear at zero-crossing is positive.....   | 41 |
| Figure 3.32 - Seasonal scatter plot of shear at zero-crossing versus peak delay.....  | 41 |
| Figure 4.1 - General model of CCCs inversions. Near the bed (red) decelerates and changes direction first. Near the surface present higher acceleration (slope) and inversion duration is very similar in both layers.....                  | 44 |
| Figure 4.2 - Three-layer vertical velocity (m/s) profile. Depth average velocities (black line), Near bed (red line) and near the surface (green line). Black arrow indicates the event of 16/11/2008 to exemplify an inversion Type C..... | 45 |
| Annex A.1- PCA applied to all parameters. Parameters loadings on the 2 maximum variance components.....   | 53 |
| Annex A.2 PCA applied to all parameters. Scores divided in seasons. ....  | 53 |

## **List of Tables**

|   |    |
|---|----|
| Table 2.1– Number of samples together with CCCs events for the Seasonal and bimonthly periods defined here..... | 15 |
|---|----|

## **List of Abbreviations**

AH – Azores high pressure cell

APG – Alongshore Pressure Gradient

CCCs – Coastal Counter-Currents

CSM – Cape Santa Maria

CSV – Cape Saint Vincent

GC – Gulf of Cadiz

SG – Strait of Gibraltar

SST – Sea Surface Temperature

STD – Standard Deviation

# 1. Introduction

## 1.1 Motivation

At the northern margin of the Gulf of Cadiz (GC), poleward currents (from east to west in the GC) exists in turn with the coastal upwelling jets of equatorward (from west to east in the GC) direction. They are referred in the literature as “Coastal Counter-Currents” (CCCs) (Fiúza, 1983; Relvas and Barton, 2002). CCCs have been reported to be responsible for delivering warm waters within the inner shelf with a sharp temperature increase up to 3-5°C in summer (Relvas and Barton, 2002). According to Garel *et al.* (2016) CCCs are a frequent feature of the inner shelf circulation (42% of the time observed), and no distinct preference for winter or summer months.

The physical drivers that control the development of CCCs in the GC remain largely speculative due to scarce long-term hydrodynamic measurements. Garel *et al.* (2016) stressed the need to assess the setup of CCCs at an event scale. In particular, due to the lack of detailed characterization, CCCs are treated as if they were generated by the same process, while it might not be the case.

In this sense, a more detailed and over time-assessment of the development of CCCs (i.e., at the time when the flow turns from equatorward to poleward) should contribute to the identification and understanding of the main driving forces involved.

The knowledge of CCCs - and the inner shelf circulation in general - is of interest of physical-chemical oceanography for numerical model setup and validation, to understand and predict contaminants transport. Furthermore, nutrient and planktonic organisms dispersion, are of interest for marine biology.

## 1.2 The Gulf of Cadiz

The GC is an embayment located between the north-western African coast and the southwestern tip of Iberian Peninsula (Figure 1.1). Its eastern boundary is defined by the Strait Gibraltar (SG) where denser waters of Mediterranean origin are exchanged and partially

mixed with Atlantic waters (Price *et al.*, 1993). The westernmost limit of the GC is marked by a sharp change in the coastline direction, the Cape St. Vincent (CSV).

The region is under influence of the Azores high pressure cell (AH) and its seasonal fluctuations (Chase, 1956). In summer, the AH is stronger and the pressure gradient with Iceland low pressure cell is not pronounced, leading northern winds to blow steadily on the west coast of Iberian Peninsula creating conditions for upwelling events. Due to Ekman's transport, surface waters are transported offshore and cold bottom waters rise in response. The Portuguese upwelling zone (Stevenson, 1977) is defined by a front of strong temperature contrast that can reach 30-50 km offshore in weak upwelling events, or 100-200 km in strong events (Fiúza, 1983).

Local features, such as the coastline discontinuity of CSV and mountains chains (Fiúza 1983; Relvas and Barton 2002; Sánchez *et al.*, 2006), may divert the northern winds direction to westerlies in the south coast, also creating conditions for upwelling in this region.

Contrarily, in winter, AH becomes weaker by its center displacement  $\approx 10^\circ$  south, culminating in gradient intensification with Iceland low. This winter set up favours winds to blow from east or southeast (Chase, 1956).

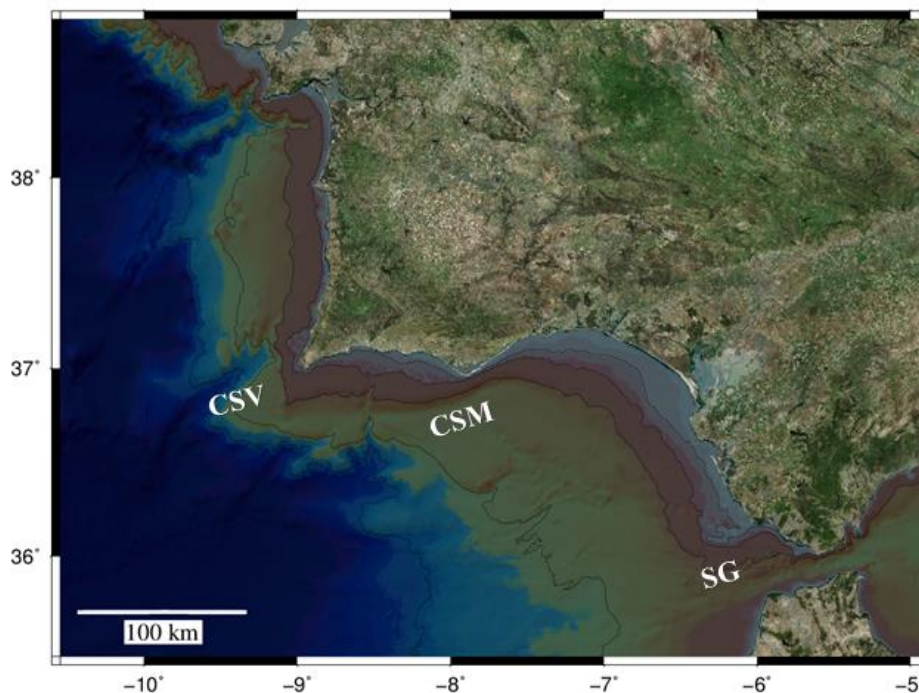


Figure 1.1- Area of interest, isobath 25m, 50m, 200m, 1000m and 2000m. Cape São Vincent (CSV) and Cape Santa Maria (CSM). Strait Gibraltar (SG).

### 1.3 Definition of coastal counter-currents

CCCs are defined as poleward flows that counter force equatorward flow generated in the western coast of Portugal.

CCCs are known to cross the entire GC northern margin (southern coastline of Portugal and Spain) and may turn clockwise around Cape São Vincent progressing up to 110 km northwards along the west coast (Relvas and Barton, 2002). In summer months, they are associated to the propagation of warm water along the southern coast (Garel *et al.*, 2016; Relvas and Barton, 2002, 2005; Sánchez *et al.*, 2006), while during winter this feature is not present (Garel *et al.*, 2016).

This poleward flow occurs in a narrow band (15-20 km) restricted to the inner shelf (Criado-Aldeanueva *et al.*, 2006; Relvas and Barton, 2005) and has the capacity to move previously upwelled waters offshore creating a high contrast temperature across the northern margin of the basin (Figure 1.2).

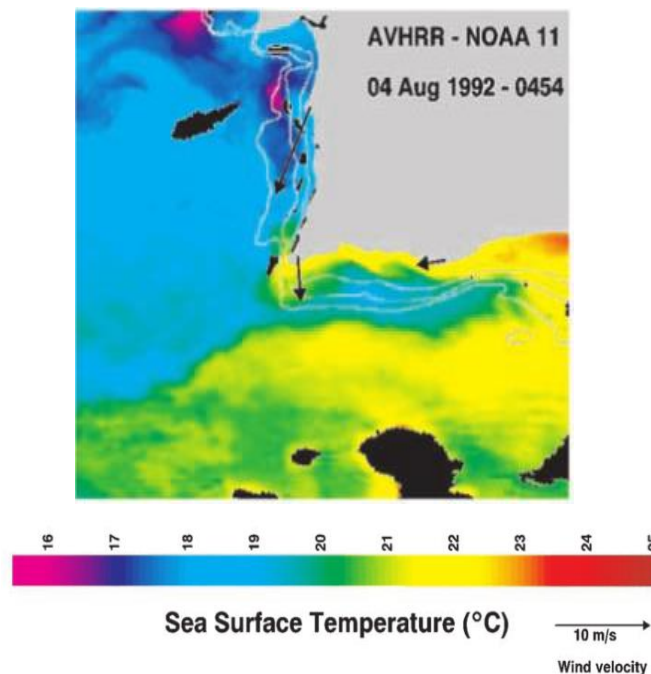


Figure 1.2 - Satellite SST adapted from Relvas and Barton (2005).

Using a multi-year (2008–2014) time-series, constituting  $\approx 18$  months of hourly records, Garel *et al.* (2016) found no seasonality. Poleward flows, were recorded up to  $0.4 \text{ m s}^{-1}$  (depth-averaged value) in accordance with Relvas and Barton, (2005). The mean duration of CCCs events were 3 days, but events lasting up to 15 days were also observed.

Local winds fail to explain the development of CCCs, although it has a clear influence on its duration and velocity. CCCs are seemingly better correlated with large-scale wind characteristic of the upwelling system (Garel *et al.*, 2016; Sánchez *et al.*, 2006).

Garel *et al.* (2016) showed that this current is mainly alongshore and barotropic. Its cross-shore component is characterized by a two-layer structure that favours transport offshore through the bottom layers, typical of downwelling conditions. While upwelled waters are typically nutrient rich, downwelling is expected to reduce nutrient availability. In fact, Navarro *et al.* (2006) and Rosa (2016) reported nutrient decrease coinciding with CCCs events. However, this cross-shore flow is weak, and only the long-shore velocity component is considered in the present study.

#### **1.4 Development of CCCs**

The mechanism involved in the development of CCCs in the GC largely speculative due to scarce long-term *in situ* hydrographic measurements. By contrast the region of Santa Barbara Channel had been the focus of extensive observations (Harms and Winant, 1998; Melton *et al.*, 2009; Washburn *et al.*, 2011). This region is very similar with the GC in terms of morphology and wind characteristics making it a good example for comparison. In particular, this region registers CCCs as a recurrent feature, with similar velocities of propagation at  $0.46 \text{ m s}^{-1}$  and a similar cross-shore behaviour (Washburn *et al.*, 2011).

Melton *et al.* (2009) and Washburn *et al.* (2011) showed that CCCs are very well correlated to Alongshore Pressure Gradients (APG) caused by differences in sea level along the coast and to relaxation of equatorward winds. These winds opposes the APG force, when those relaxes APGs becomes the main force, triggering CCCs.

Similarly, In the GC Relvas and Barton (2002) using satellite Sea Surface Temperature images (SST), time series of sea level height (1982-1991 at four tide gauges), wind velocities, and nearshore sea surface temperature records, suggest that CCCs are driven

by a background APG whose effect is augmented or diminished by wind forcing. These authors also suggest that the recirculation of Atlantic waters entering the GC proposed by Mauritzen *et al.* (2001), can be responsible for reinforcement of the surface tilt.

Another interesting feature is the pool of warm water near Guadalquivir river mouth, present in summer SST images. Apparently, the main source of heat is land. Due to tide amplitude and negligible river discharge during spring/summer, few km<sup>2</sup> of marsh can be flooded twice a day, and enhance energy absorption in these shallow areas. This will generate a buoyant plume of water that will contribute to the sea level slope by density effect (García-Lafuente *et al.*, 2006).

In winter the APG is expected to diminish in relation to the seasonal change in wind conditions (Relvas and Barton, 2002); furthermore, the pool of warm water in the Gadalquivir mouth becomes a source of cold water due to the increase of fresh water discharge (Gabriel Navarro and Ruiz, 2006). Nevertheless, poleward flows are still present in winter 43% of the time (Garel *et al.*, 2016).

It is important to note that most of these works summarized here were based on remotely sensed SST climatological data or short duration shipboard surveys. Analyses of *in situ*, long-term measurements like the one performed by Garel *et al.* (2016) are essential to assess the mechanisms involved on the process of generation of these currents.

## **1.5 Interaction with the open sea circulation**

Upwelled water along the west coast causes the surface dynamic height to decrease towards the coast and consequently creating a pressure gradient with the same orientation. By geostrophic adjustment, where pressure gradient force is balanced by Coriolis effect, a flow develops in the southward direction (the so-called “upwelling jet”). Generally this flow turns eastward around CSV, but less usually, it has been observed turning westward or continuing southwards (Relvas and Barton, 2002). Water that had been upwelled in the south coast may merge into the jet that turned around the cape and deliver cold waters into the GC basin (Sanchez and Relvas, 2003).

Several studies have reported a quasi-permanent cyclonic circulation in the central part of GC (Criado-Aldeanueva *et al.*, 2009; García-Lafuente *et al.*, 2006; Garcia *et al.*, 2002;

Sanchez and Relvas, 2003). Vargas *et al.* (2002) performed an Empirical Orthogonal Function analysis to identified spatial patterns of satellite SST images in the GC. They also observed a frequent warm region in the southern part of the area of study.

In winter, the cyclonic eddy becomes weaker and displaces southward. This eddy is thought to act as a connection of the jet of upwelled waters with the SG (Peliz *et al.*, 2009; Peliz *et al.*, 2007).

Mauritzen *et al.* (2001) states that recirculation is required in the northern margin of GC due to the excess of Atlantic waters entering the SG. The excessed water that is not needed to enter the strait, gains salinity from the underlying Mediterranean outflow and flows poleward over the continental shelf.

García-Lafuente *et al.* (2006) defined the circulation of the inner shelf in the GC composed by two cyclonic gyres that can be connected when wind conditions are favourable: The first gyre, located in the eastern side, is a result of the geostrophic adjustment due to the density gradient created by the equatorward cold jet and warmer waters of the inner shelf. The cyclonic circulation becomes complete when this current is forced to turn south-westwards (partially at least) and merge again within the equatorward flow due to the presence of Cape Santa Maria. The second gyre, located in the western part, seems to be related to the response of wind stress in the region of CSV (Mazé *et al.*, 1997). A more recent work of Relvas and Barton (2005) identified the same structure flow and justified, using computed surface dynamic heights, that it was a surface signature of a deeper Mediterranean water eddy (*i.e.* Meddies).

## 1.6 Objectives

In order to categorize CCCs setup (*i.e.*, “inversions”, defined hereafter strictly as the moment of maximum acceleration in the equatorward direction preceding the flow direction change until the moment of maximum acceleration in the poleward direction), and bring more evidence on their controlling mechanisms, multi-year current data were collected with a bottom-mounted Acoustic Doppler Current Profilers (ADCP), between 2008 and 2017, in the south Portuguese inner shelf.

The main goal of the present research is to exploit this dataset in order to characterize the variability of inversion patterns (and thus identifying various types of CCCs) by performing a detailed analysis of the along-shore flow structure during these events. Important to be mentioned, the reversal phenomena (defined here as the turn of the flow from poleward to equatorward) behaviour is not under the scope of this study. Inversion types were inferred by the mutual analysis of several parameters extracted from inversions. It is further proposed to explore if the identified types of inversion reflect the action of potential responsible forces for the development of these currents.

## 2. Materials and methods

### 2.1 Data

The time-series used to reach the proposed objective are composed by a multi-year current velocity recorded at Armona station ( $37^{\circ}0,648' N$ ;  $7^{\circ}44,480' W$ ) at 23m depth (Figure 2.1), using a Workhorse 600kHz, TRDI ADCP bottom mounted on top of a concrete artificial reef of 1.4 m height.

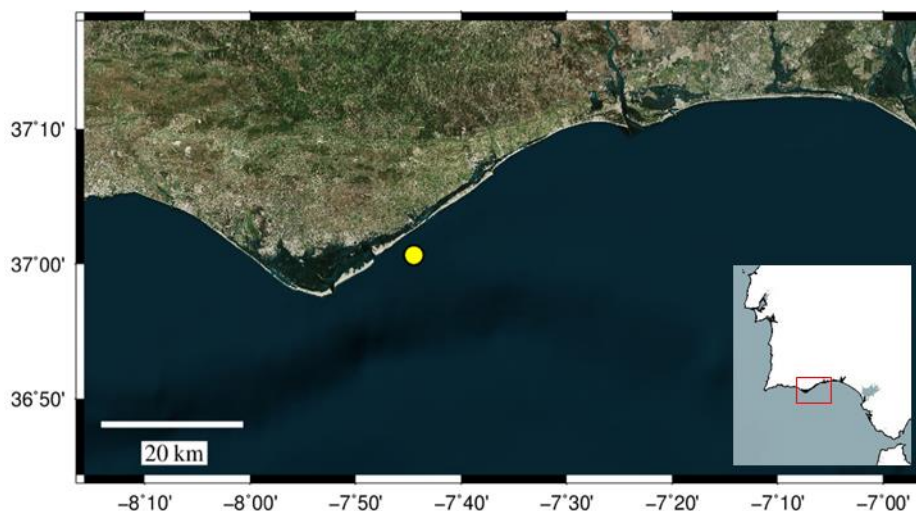


Figure 2.1 - ADCP location (yellow circle).

A total of 13 deployments were performed at different times of the year (Figure 2.2),

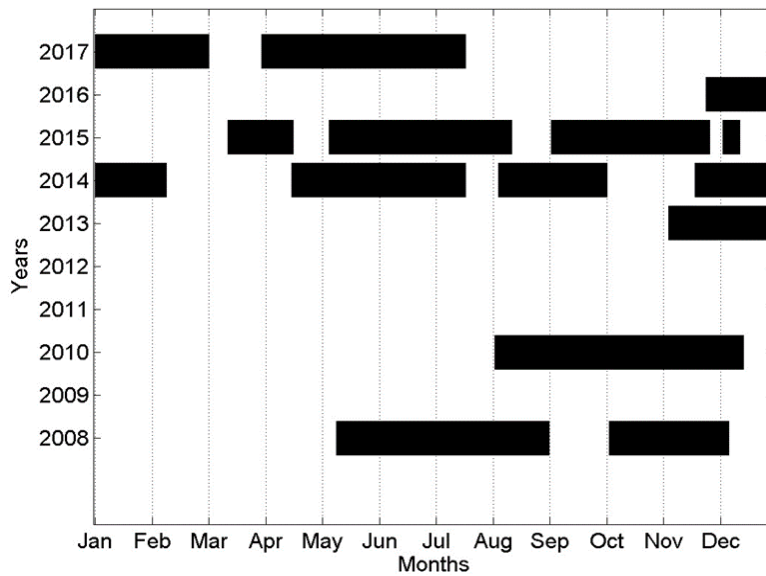


Figure 2.2 - Deployments duration, black bars indicating each deployment duration.

and 22153 samples were recorded.

From 2008 until 2017, the years of 2009, 2011 and 2012 were not sampled while 2008, 2014 and 2015 were the years with more samples.

It is clear that the second half of the year present a higher sampling coverage and thus results must had been analysed carefully considering the coverage patterns, especially when considering the month of March.

The ADCP device (Figure. 2.3) is used to record water flow velocity in three dimensions, near bed temperature and pressure. Two independent sensors measure temperature and pressure. Velocity is measured by emitting an acoustic signal that is reflected by particles present in the water. By receiving back, the signal, and verifying the frequency changes it suffers from the reflection, the velocity of the particles can be calculated (Doppler effect). This velocity is considered as equal to the flow velocity. The equipment has an internal compass and data are recorded in orientation of N-S W-E Cartesian coordinates. Velocities are recorded at different depths (cells) along the water column. The width of each cell is dependent of the set up used for each deployment.

Data were recorded at hourly intervals, along cell sizes of 0.5 m, (except for deployment of October-December in 2008 where the cell size was 1 m).



Figure 2.3 - ADCP Workhorse 600kHz, TRDI

## 2.2 Data processing

Once the data had not been through any processing, the first task to be accomplished was the preparation of the time-series for their analysis.

The processing of the data was performed by Matlab (v.2014) script that consisted of:

1- Remove cells with invalid data (out of water or contaminated by the surface boundary) – The number of valid cells can vary due tide, waves or particles and needed to be corrected. The criteria used for removing invalid cells was the signal intensity. When signal suffer a sharp increase in intensity (due to the influence of the water surface) cells above this level were discarded. Figure 2.4 exemplifies a set of measurements where blue lines represent

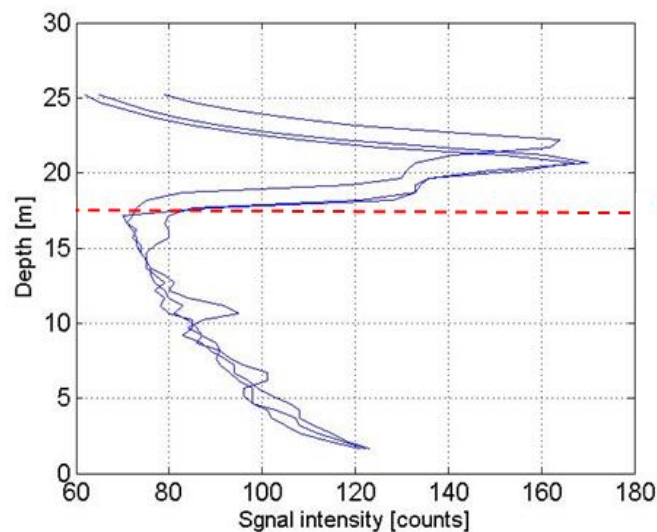


Figure 2.4 - Intensity of signal along the water column.

the signal intensity and dashed red line highlight the threshold mentioned above. In this case, cells above 17 m were flagged as invalid. Validated cells data were rotated in cross-shore and along-shore components using the angle of maximum variance ( $22.9^\circ$ ). A simple linear regression using the raw velocities showed the angle of maximum variance. Positive alongshore current velocities represent W-E direction and negative, E-W.

3- Remove tidal signal from current records – The tidal cycle is semi-diurnal in the region, and therefore every 12 hours 25 min a cycle is complete. These oscillations have an effect in the horizontal movement of the water and have to be removed using a Butterworth low-pass filter using a 40 hours cut-off period. An example is presented in Figure 2.5.

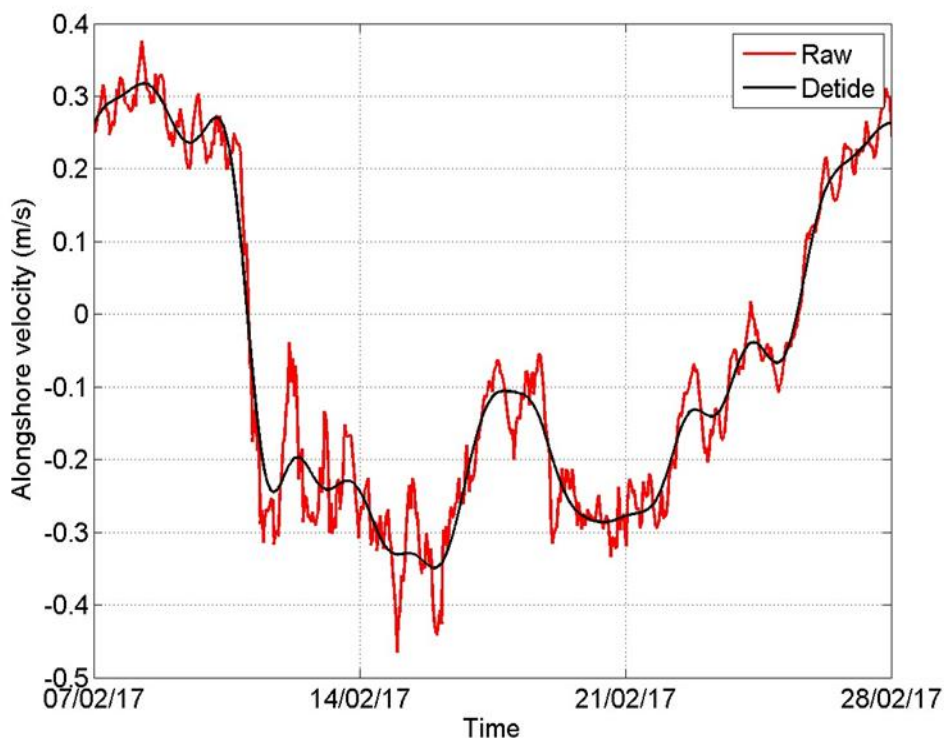


Figure 2.5 - Current velocity. Raw (red) and detide (black) using Butterworth low pass filter 40 h cut-off period. Negative values are poleward.

4- Extract the near surface, depth average and near bed layer velocities from the detide time series (Figure 2.6).

Near surface was defined to be the mean value of the 2 uppermost valid cells. Averaging is done to reduce the standard deviation (i.e., small errors affecting measurements

at each cell). Depth average was defined to be the mean of all cells and near bed was the mean of the 2 cells closest to the bottom.

Data was compiled in a catalogue based in all the ADCP data available. It was built on the definition of parameters defined here (see next section) applied for the three water layers (near surface, depth average and near bed).

The construction of the catalogue allowed to group all identified inversions and their parameters and further the creation of inversion categories by assessing the distribution of parameters.

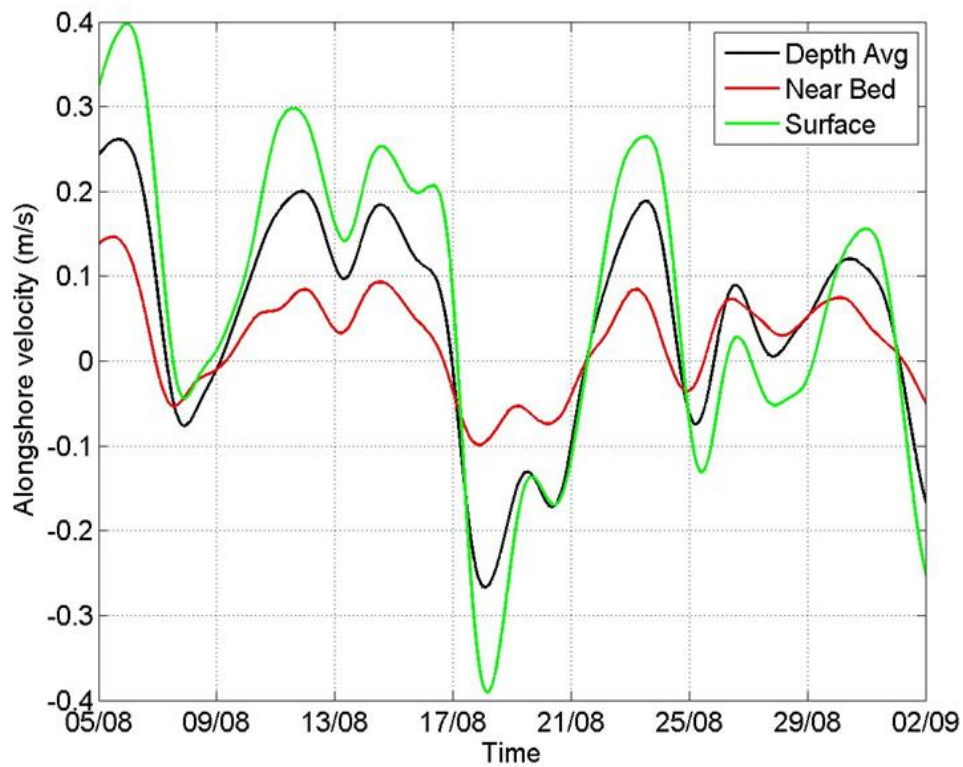


Figure 2.6 - Example of detide surface, depth average and near bed velocities.

### 2.3 Parameters definition

Peak delay - A peak is defined here, as the closest significant peak before and after direction change. It is chosen when the first derivative of the velocity signal is zero. It is the

point of maximum velocity preceding and after signal zero-crossing. Between these points, it is assumed that the driving forces of inversions are predominant.

Peak delay is measured in hours, this parameter quantifies time interval between peaks of surface and bed layers before inversion (Figure 2.7). Positive values indicate that near bed layer started to turn (decelerate) before the near surface layer. Negative values represent the opposite, near surface layer started to turn before near bed layer.

For few cases, the selection of the peak delay was a complicated task, and peaks could have been chosen differently. A specific peak (first derivative of the velocity signal equals zero), could have been preceded by another peak where the velocity signal was greater making the selection of the peak difficult. However, doubtful peak selection was not a recurrent situation and main results would not suffer critical changes.

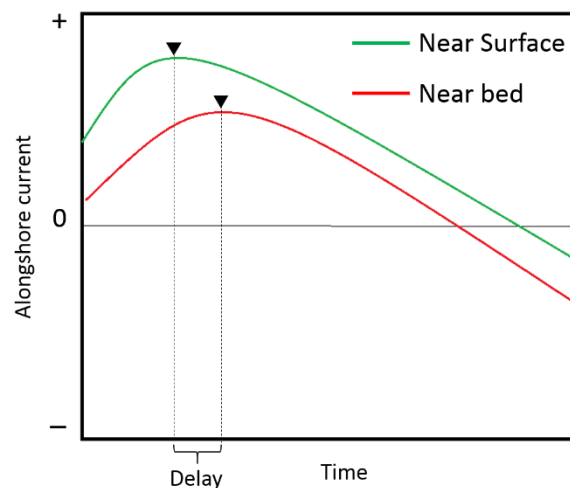


Figure 2.7 - Peak delay scheme. Black triangles indicate peaks (first derivative = 0). Near surface (green), Near bed (red).

Inversion Duration - Time interval in hours between the peaks before and after zero-crossing. It measures the time interval of when the velocity started to decrease in the equatorward direction until it stopped to accelerate in the poleward direction (Figure 2.8). This parameter was measured for near surface and near bed layers.

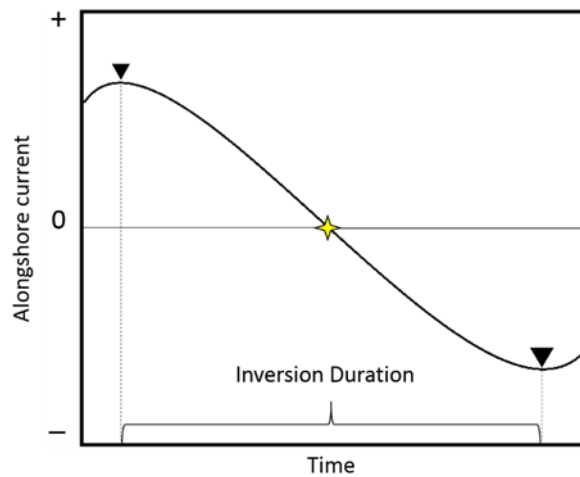


Figure 2.8 - Inversion duration scheme. Black triangles indicate peaks before and after zero-crossing (yellow star)

Shear at zero-crossing – Shear is calculated from the velocity differences between the near surface layer and the near bed (surface minus bed) at the time when the average velocity changes signal (Figure 2.9). Positive values of shear indicate that the near bed layer inverted before the near surface layer and negative values indicates the opposite, near surface changes direction before the bed.

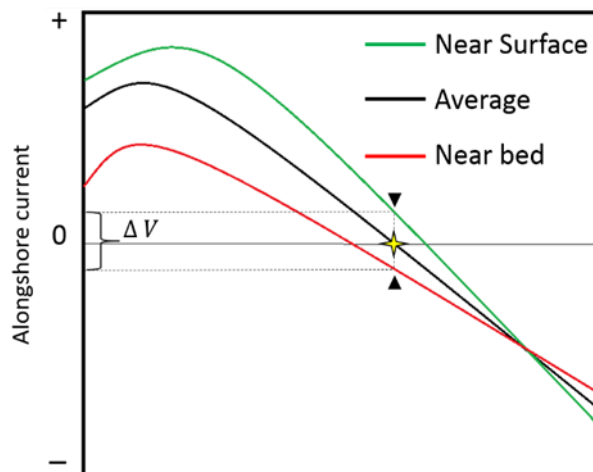


Figure 2.9 - Shear at zero-crossing scheme. Zero crossing in the average layer is indicated by the yellow star. Black triangles indicate the velocity values for the Near surface/bed layer where velocities differences are calculated from.

Slope at zero-crossing ( $\Delta v/\Delta T$ ) – Velocity slope computed from points 1 hour before and after the inversion in the different layers: near surface and near bed (Figure 2.10). It quantifies the acceleration of current.

Slope will be assessed using the definition of high slope and low slope. It is defined here as the mean value  $\pm$  standard deviation (STD) of all data distribution for each layer.

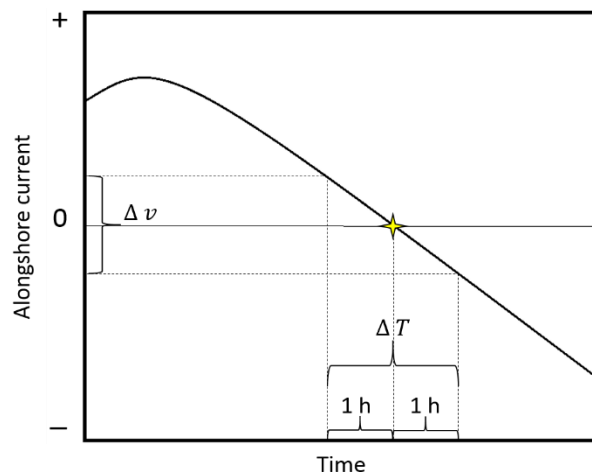


Figure 2.10 -- Slope at zero-crossing scheme. Current's acceleration computed from the velocity variation 1hour before and 1 hour after zero-crossing (yellow star).

Slope differences – Slope at zero-crossing differences between near surface and near bed layers (surface minus bed). Positive values of Slope differences mean that near bed layer has a higher acceleration than near surface, and negative values the opposite, near surface layer has a higher acceleration than near bed.

Some cases where slope differences resulted in a positive value, were also recorded in a doubtful situation. Sometimes, the moment of direction change of surface layer, was very close to the velocity maximum or close to a short velocity deceleration-acceleration moment. In both situations slope at zero crossing becomes close to zero, even though the total inversion slope is more accentuated. This few cases resulted in the most extreme positive values presented here ( $>1 \times 10^{-6}$ ). Again, these specific cases do not affect the main findings of the slope related parameters.

Slope differences will be assessed using the definition of positive and high negative slope differences, defined here as mean minus STD.

## 2.4 Temporal periods and seasonal definition

The data were sampled during different periods over several years, and therefore, the analysis will be performed using different periods to verify any variability in the dataset. Firstly, each parameter will be analysed considering all the data. Secondly, variability will be checked seasonally and at last using bimonthly time scales.

Seasonal variations were analysed considering the typical seasons in the region, i.e. winter (from December until February), spring (from March until May), summer (from June until August) and Autumn (from September until November). Bimonthly variations were analysed by selecting groups of two months as: January – February, March – April, May – June, July - August, September - October, November – December. These groups were selected since some of these months present similarities that could be hidden in the seasonal analysis. For example, the characteristics of the month of June, in some parameters, are closer to May than to August, although it belongs to the summer season.

The Seasonal periods defined here, present comparable number of samples and number of CCCs registered events for most of the periods (Table 2.1). For the bimonthly analysis, the number of samples of the March-April period should be assessed carefully, as it presents only 1976 samples and 7 CCCs events.

Table 2.1– Number of samples together with CCCs events for the Seasonal and bimonthly periods defined here.

| <b>Period</b> | <b>Number of Samples</b> | <b>CCCs events registered</b> |
|---------------|--------------------------|-------------------------------|
| Winter        | 5140                     | 20                            |
| Spring        | 4616                     | 24                            |
| Summer        | 7532                     | 34                            |
| Autumn        | 7524                     | 42                            |
| Jan - Feb     | 2350                     | 10                            |
| Mar - Apr     | 1976                     | 7                             |
| May - Jun     | 5520                     | 29                            |
| Jul - Aug     | 4652                     | 22                            |
| Sep - Oct     | 4354                     | 24                            |
| Nov - Dec     | 5960                     | 28                            |

## **2.5 Statistical and parameters integrative analysis**

Parameters distribution were analysed using a boxplot representation. The main information used for the analysis was regarding the mean value, the STD and the interquartile range (IQR). Extreme values were not considered outliers, they rather represent extreme events.

Normality (Kolmogorov–Smirnov test) and homogeneity of variances (Levene’s test) were verified prior to statistical comparisons among seasons and bimonthly periods.

To identify if seasons and bimonthly periods come from an identically distributed population, the performed comparisons were based on the non-parametric Kruskal-Wallis test, and on a non-parametric Dunn post-hoc multiple comparisons (Dunn, 1964).

The best relationship observed among parameters was obtained visually using scatter plots of Peak delay and Shear at zero-crossing. Inversions types were created considering the sign of the parameters, and all 4-possible combination generated the 4 types proposed.

A multivariate analysis (Principal Component Analysis – PCA) was performed using the software STATISTICA 8.0, in order to integrate the relevant parameters and assess their potential seasonal correlation. Results obtained using this technique showed no meaningful variance of parameters in relation to seasons (see annex A).

## **3. Results**

### **3.1 Data overview**

The analysis of the data-series allowed the observation of 120 current inversions during the 13 deployments performed ( $\approx 9$  inversions per deployment in average).

In the poleward direction, velocity can reach up to 0.41 m/s in the average layer, the mean peak velocity is 0.17 m/s. Near the surface CCCs maximum is 0.65 m/s and mean peak velocity equals to 0.21 m/s. Near the bed velocity can reach up to 0.27 m/s with the mean peak velocity reaching 0.09 m/s. CCCs events can have one or more velocity peak during its duration. On average, a CCCs event, develop 1.5 peaks

CCC's events occurs in average 3.35 times per month. The longest CCC's registered last for 534 hours ( $\approx 22$  days) on the 15th of October until the 6th of November in 2015.

## 3.2 Parameters results

### 3.2.1 Peak delay

The Peak delay distribution represented in Figure 3.1, shows that positive peak delay, where near bed layer started to turn before the near surface layer occur more often 79%, against 21% of negative peak delay where near surface started to turn before the bed layer. For most of the cases (60.8%) the delay is less than 5 hours, 44.2% occur from 0 to 5 hours and 16.7% occur from 0 to -5 hours.

Peak delay can range from  $\approx -15$  hours to  $\approx 27$  hours and the mean value is 3.65 hours with STD equals to 6.13 hours. Positive peak delay is on average 5.6 hours with 4.97 hours STD and negative peak delay is on average -3.73 hours with STD 4.24 hours.

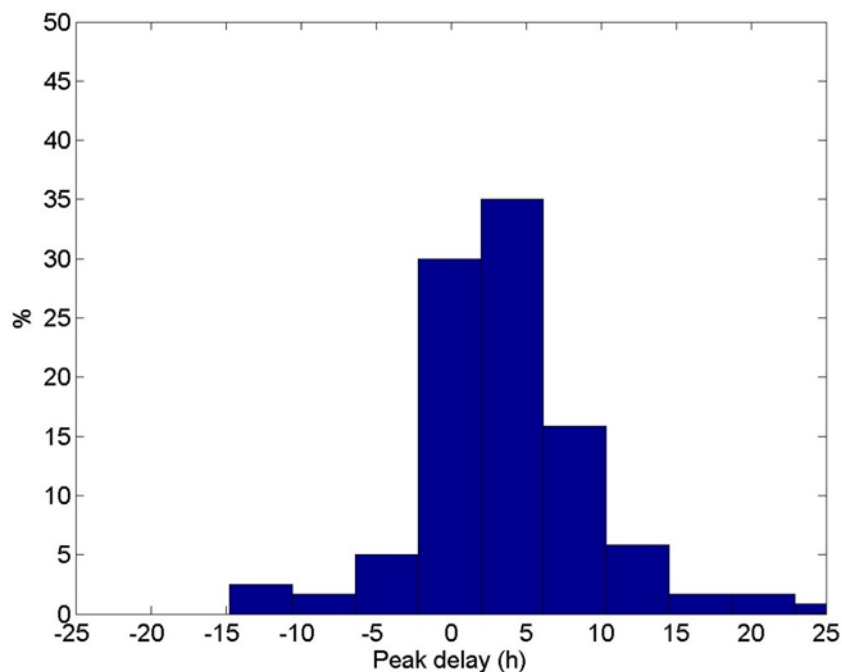


Figure 3.1 - Peak Delay (in hours) all data distribution

3.2.1.1 Seasons

Along the year the mean value of peak delay is highest in spring and decreases towards winter together with the variability of the data. Note that the IQR in winter is approximately the half of spring (Figure 3.2). In winter peak delay is 0.26 hours on average with STD 3.86 hours, in spring 5.88 hours (STD 7.19 hours), in summer 4.6 hours (STD 5.11 hours), in autumn 3.22 hours (STD 6.54 hours).

During winter, extreme values are not registered as it is in the other seasons, 85% of the cases peak delay is within the range of -5 to 5 hours.

Seasons showed statistically significant differences among themselves (Kruskall-Wallis test  $P > 0.05$ ) and the post hoc test indicated that winter differs more from spring and summer while autumn is a transitory period.

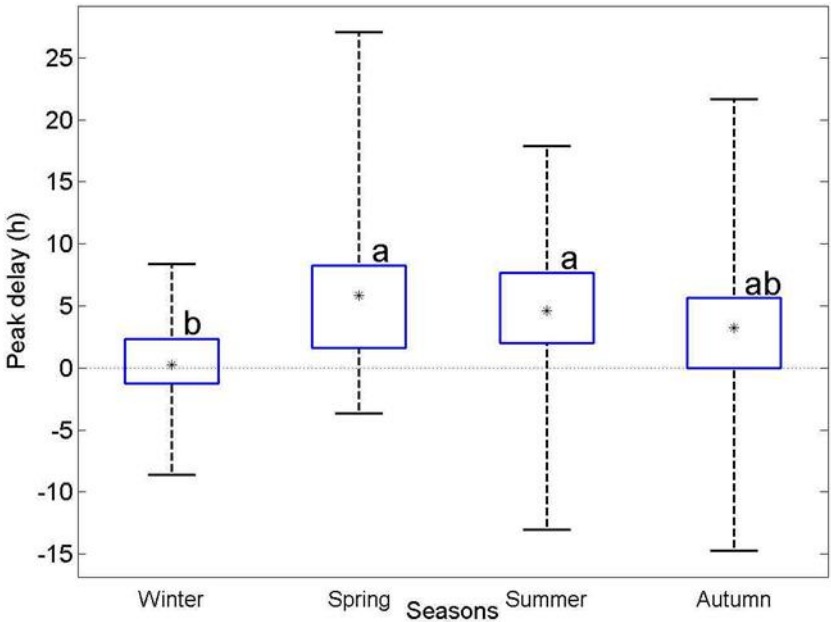


Figure 3.2 - Peak delay (in hours) seasonal distribution. Mean represented by asterisks and letters indicates groups differences obtained after Kruskal-Wallis test ( $P > 0.05$ ) and Dunn post hoc comparisons.

Winter present the lowest percentage of positive peak delay (60%). While spring present 83 %, summer 91% and autumn 76% (Figure 3.3).

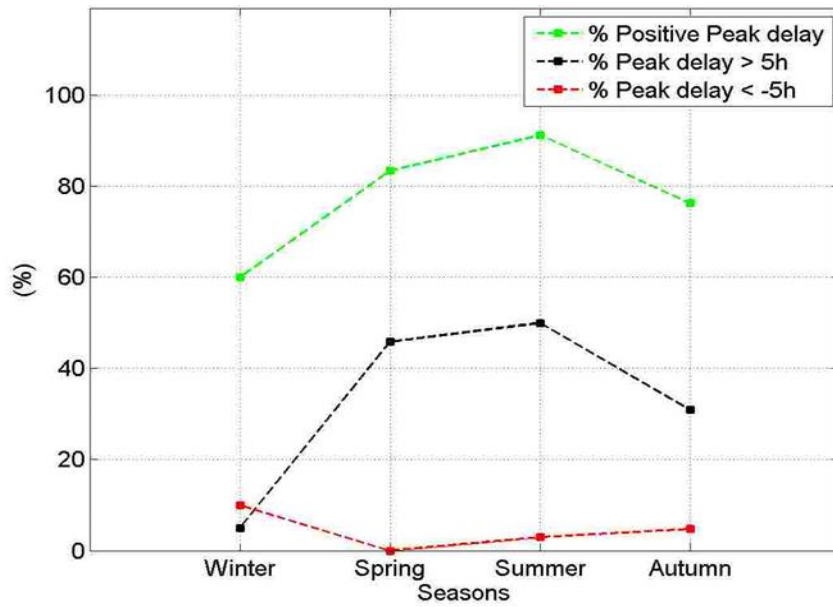


Figure 3.3 Percentages of positive peak delay (green), peak delay > 5 hours (black), together with percentage percentages of peak delay < -5 hours (red) for each season.

Peak delay > 5hours happens with more frequency in the summer months (50%) and seldom registered in winter (5%). Peak delay <-5 hours have much less expression, it is absent in spring, 3% in summer, 5% in autumn and its maximum occurs in winter (10%).

### 3.2.1.2 Bimonthly scale analysis

When peak delay distribution is plotted in function of two months period (Figure 3.4) the seasonal fluctuation of the mean values maintains, with higher values in spring-summer and lower in winter-autumn months.

The mean value for all periods of two months is positive except for the period of January-February (mean -0.16 hours and STD 3.83 hours). Mean is highest for the period of March-April (6.90 hours and 9.96 STD hours), for this period the variability is also the largest

(wider IQR). During May-June mean peak delay is 5.06 hours, in July-August 4.65 hours, in September-October 3.79 hours and finally November-December with a mean value (1.82 hours) and distribution similar to January-February.

Although the Kruskal-Wallis test presented a value of  $P < 0.05$  the post hoc test did not show significant differences among the bimonthly periods.

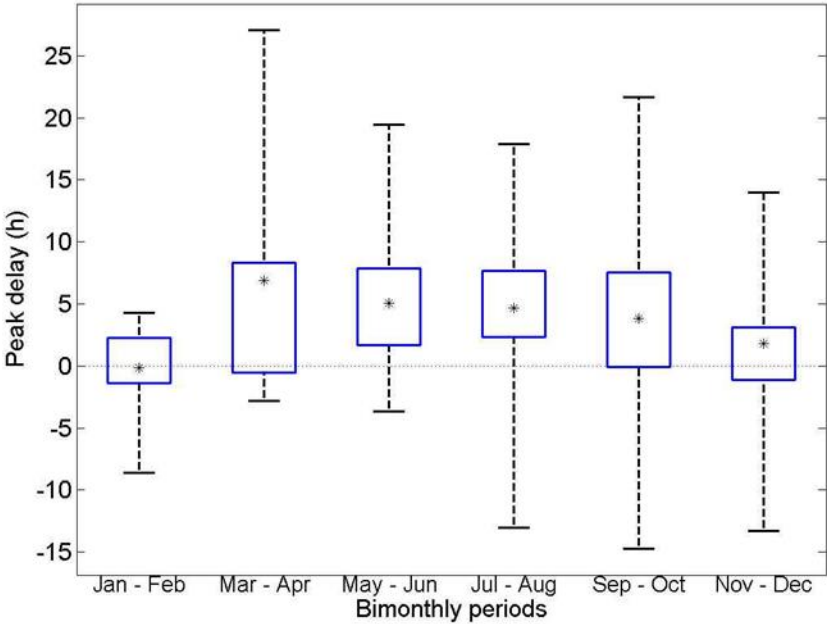


Figure 3.4 - Bimonthly peak delay (in hours) distribution. Mean represented by asterisks.

The percentage of positive peak delay is the highest in July-August (95.5%), while the lowest (40%) is registered in the period of January-February (Figure 3.5). The period of March-April present 57% of peak delay >5 hours while the period of January-February presents the highest percentages of peak delay <-5 hours (10%).

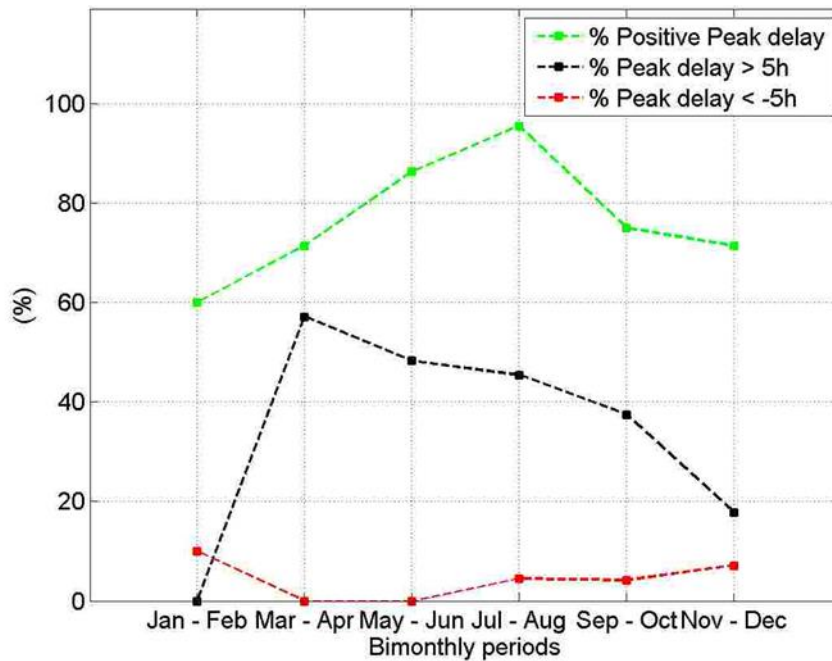


Figure 3.5 - Percentages of peak delay > 5 hours(black), together with percentage percentages of peak delay < -5 hours (red) for period of two months.

### 3.2.1.3 Summary of main observations

Peak delay analysis showed that inversions begin near the bed first, and occurs more from March to August. The period of March-April presents the highest percentages of extreme positive values of peak delay.

Negative peak delay may occur any time with relatively low frequency. It is more present from November to February, but the few extreme negative values appeared between July and December.

The analysis of this parameter highlighted that there is a strong difference in the development of the inversion between winter and spring-summer.

## 3.2.2 Inversion Duration

The Inversion duration is on average, 48.25 hours (STD 23.56 hours) in the surface layer and 48.41 hours (STD 23.1 hours) near the bed. Most of the inversions are comprised

between 20 and 50 hours as shown in figure 3.6. Near the surface 70% of the registered inversions, last less than 50 hours and near the bed 67.5%.

Both layers distributions are very similar even on their range. Near the surface inversions range from 18.43 hours up to 164.08 hours. Near the bed it ranges from 22.22 hours to 158.75 hours. For the same event of CCCs, near surface and near bed layers can present durations that can differ up to 40-50 hours one from another. These situations were rather rare and in general differences on inversion duration between layers were small.

No statistically significant differences (Kruskall-Wallis test  $P > 0.05$ ) were found in the seasonal neither in the bimonthly scale analysis of inversion duration for both layers.

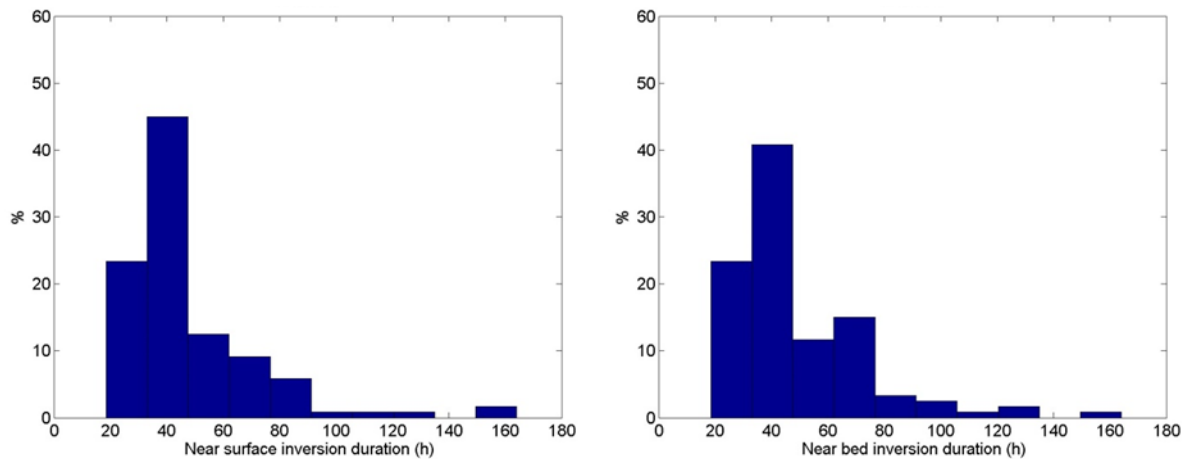


Figure 3.6 - Inversion duration in hours all data distribution. Near surface left and near bed right.

### 3.2.2.1 Seasons

Figure 3.7 represent the inversion duration distribution in function of seasons. For both layers the summer period is when the mean values of inversion duration are the highest, 55.36 hours near surface and 54.26 hours near bed approximately, 10 hours more than the other seasons. For the same period variability also increases in both layers presenting highest STD values, 34.4 and 32 hours for near the surface and near the bed layers respectively.

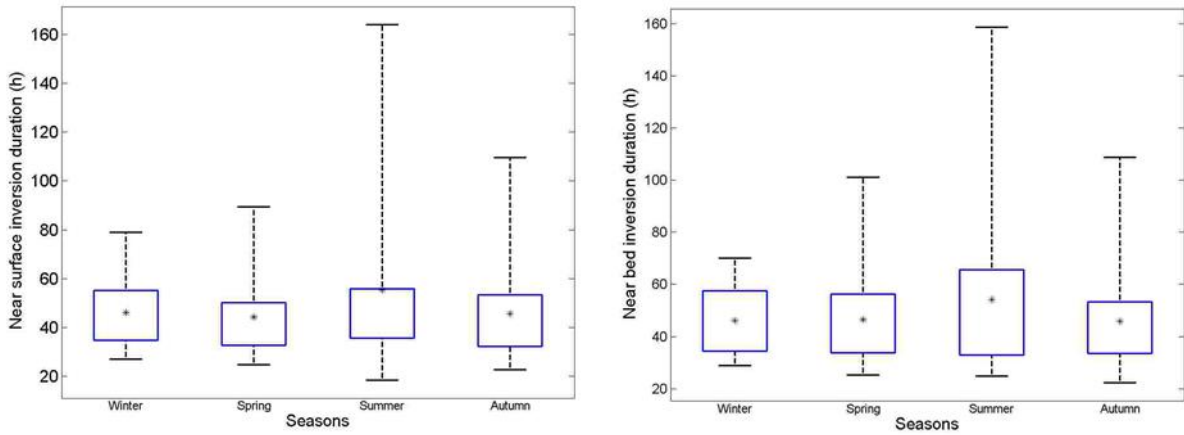


Figure 3.7 - Inversion duration (in hours) seasonal distribution. Near surface left and near bed right. Mean represented by asterisks

Figure 3.8 shows the variation on the percentage of inversion duration >50 hours and highlight the difference between the two layers. In winter it was registered 40 % near bed against 30 % near surface.

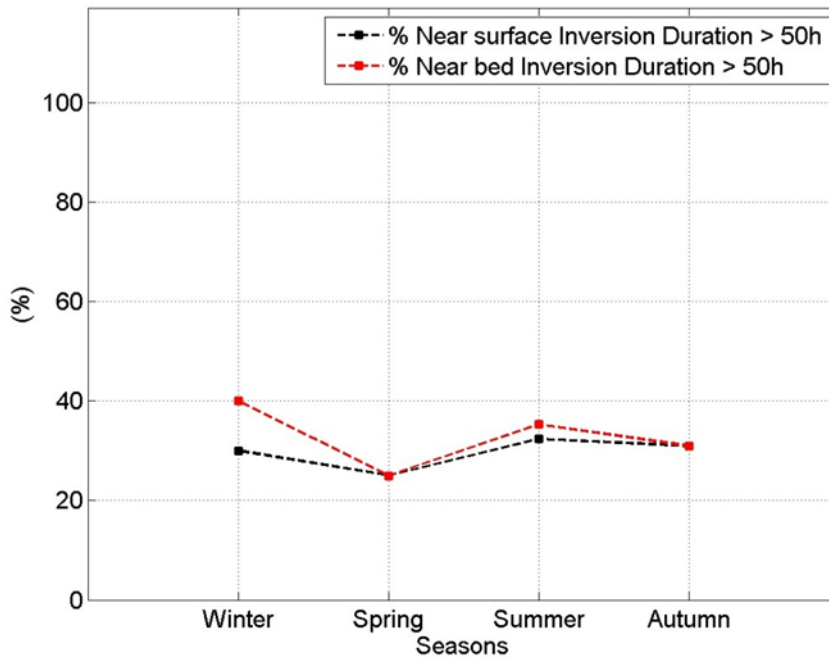


Figure 3.8 - Percentage of Inversion duration > 50 hours for each Season. Near Surface in black and near bed in red.

### 3.2.2.2 Bimonthly scale analysis

The bimonthly distribution of Inversion duration presented in Figure 3.9 shows that the highest mean values were registered in the period of May-June in both layers. Near surface the mean value reach 53.79 hours and 53.68 hours near the bed.

From July to December, inversion duration mean value and distribution do not vary much. From January to April inversion duration data tend to present lower variability values with small IQR.

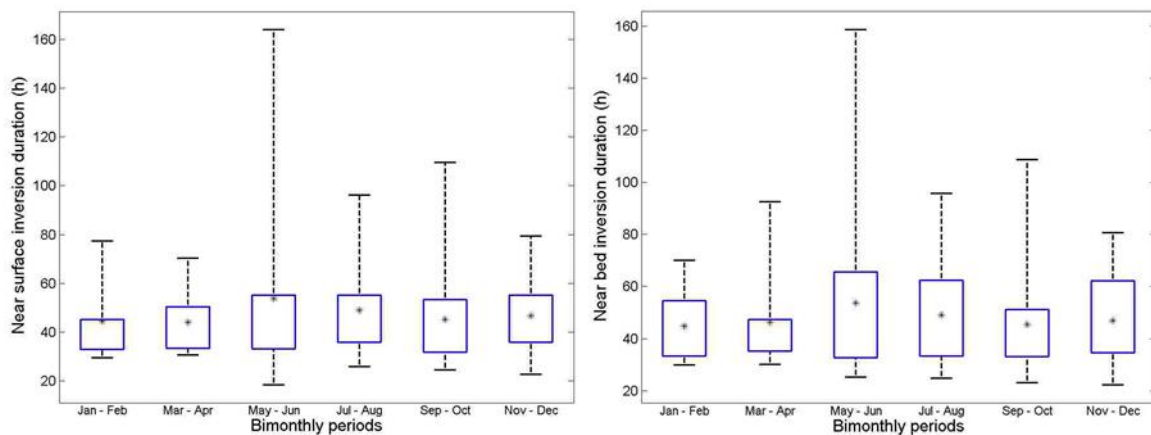


Figure 3.9 - Inversion duration (in hours) bimonthly distribution. Near surface left and near bed right. Mean represented by asterisks

The occurrence of long inversions (>50 hours) is more frequent in the period of November-December (Figure 3.10). Near the surface this period present 35.71% of long inversions and near bed 39.29%

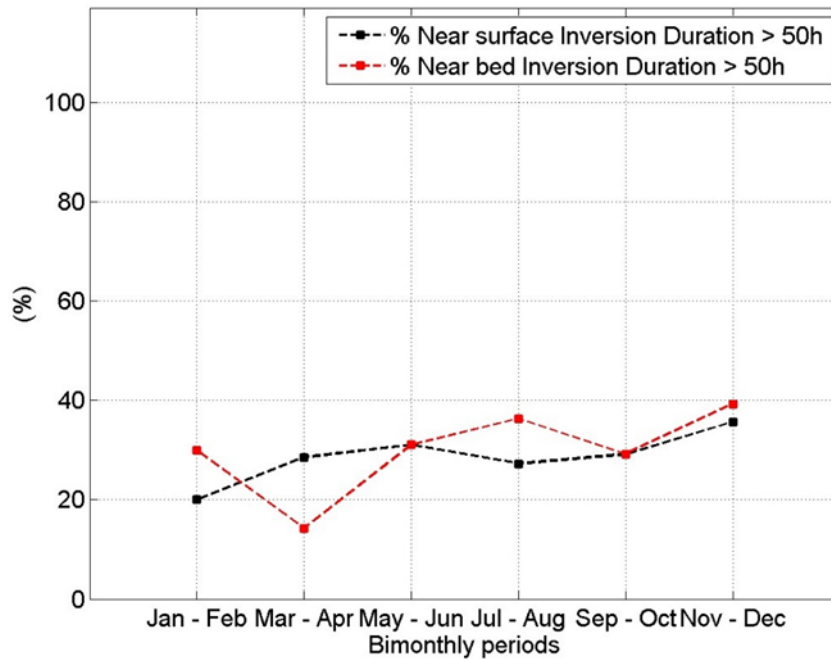


Figure 3.10 - Percentage of Inversion duration > 50 hours for each Season. Near Surface in black and near bed in red.

### 3.2.2.3 Summary of main observations

Current inversions duration is on average, two days in both layers. Inversion duration distribution is very similar among layers and no strong difference is observed between layers along the year.

In general inversions are shorter in winter months. From May to December inversion duration is more variable and generally longer.

### 3.2.3 Shear at zero-crossing

Values of Shear vary from -0.05 m/s to 0.16 m/s (Figure 3.11). The mean shear value is 0.05 m/s with STD 0.05 m/s. Positive and negative Shear occurs 77% and 23% of the time respectively.

The distribution seems to present two populations, the first ranging from -0.05 m/s up to 0.1 m/s representing 78 % and the other from 0.1 m/s up the 0.16 m/s that represent 22%

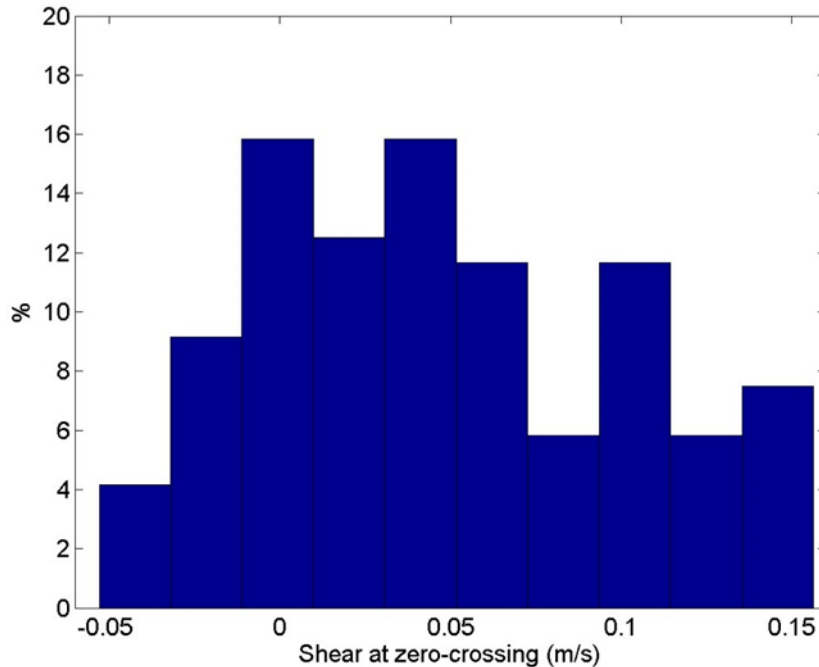


Figure 3.11 - Shear at zero crossing (m/s) all data distribution. of the total distribution.

### 3.2.3.1 Seasons

When Shear is plotted with seasonality (Figure 3.12), winter presents low values of shear, the mean is the lowest among seasons (0.02 m/s). In spring mean increases to 0.07 m/s and in summer 0.06 m/s. In autumn, the distribution is similar to summer with a slight decrease of the mean to 0.04 m/s, due to the presence of more negative shear.

Data variability are different among seasons, winter present the lowest STD (0.04 m/s) while summer the highest (0.06 m/s). STD values does not stand out much the differences among seasons, IQR shows the same relation but with differences more evidenced (0.04 m/s for winter and 0.1 m/s for summer).

Kruskall-Wallis test showed that seasons present statistically significant differences ( $P < 0,05$ ) and the post hoc comparisons indicates that spring and winter have the strong differences and a difference between spring and autumn is also observed.

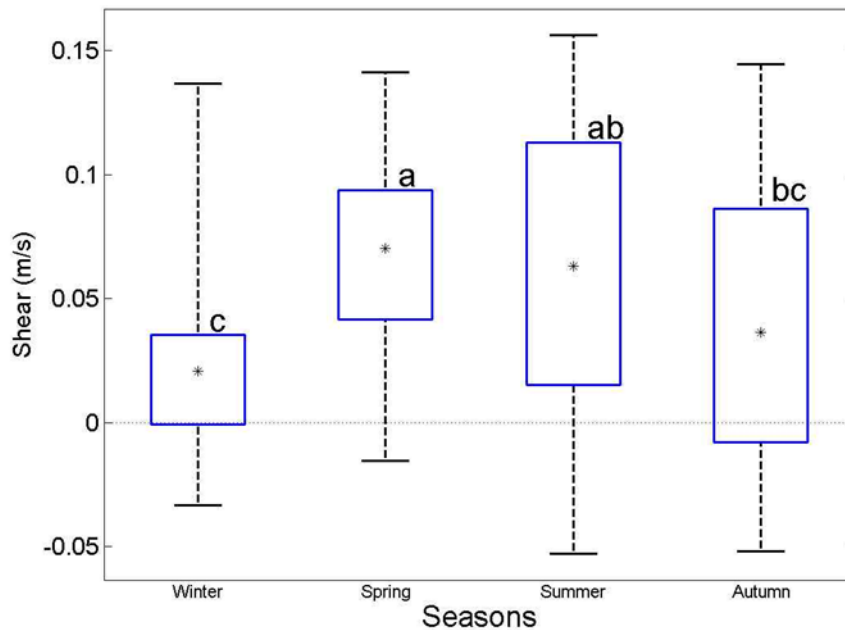


Figure 3.12 - Shear at zero crossing (m/s) seasonal distribution. Mean represented by asterisks and letters indicates groups differences obtained after Kruskal-Wallis test ( $P > 0.05$ ) and Dunn post hoc comparisons.

In Figure 3.13 is represented the percentage of negative shear for each season together with the fluctuations of the percentages of shear  $>0.1$  m/s. Winter present 30% of negative shear and percentage of shear  $>0.1$  m/s is the lowest (5%). Spring present inversions with preference to have positive shear, negative shear represent only 8%. For this period, the percentage of shear  $>0.1$  m/s is 21%. In summer 12% of the cases present positive shear and the percentage of shear  $>0.1$  m/s increases to 32%. In autumn, the presence of negative shear is the highest (36%) and the percentage of shear  $>0.1$  m/s decreases to 21%.

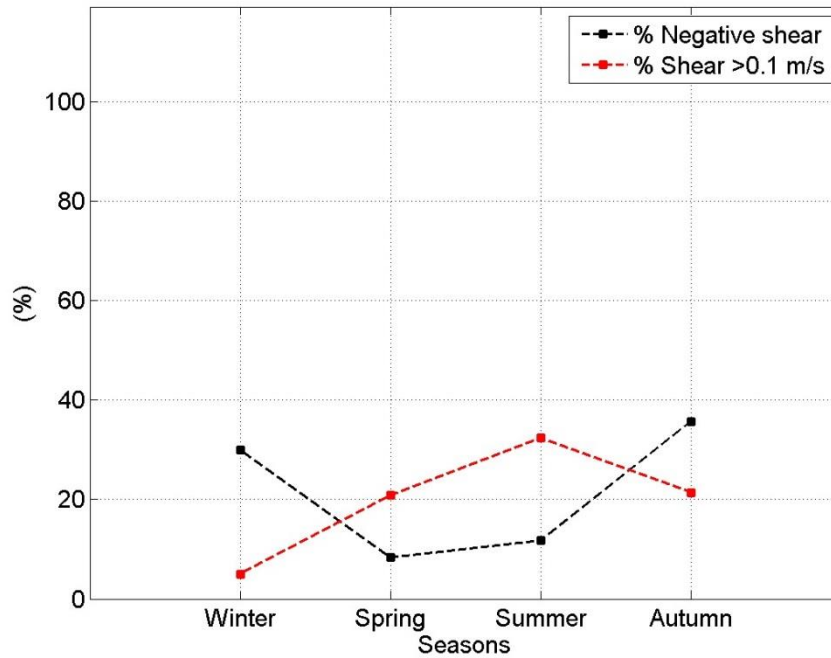


Figure 3.13 - Percentages of negative shear at inversion (black), together with percentage of shear >0.1 m/s (red) for each season.

### 3.2.3.2 Bimonthly scale analysis

The small-scale analysis of the Shear at inversion in Figure 3.14 shows that for the period between January-February, there is a high number of shear with low values (interquartile range from -0.001 m/s to 0.025 m/s), the lowest mean value (0.01 m/s) and STD is also the smallest (0.02).

For the period of March-April the mean is the highest (0.08 m/s) and decreases toward September- October 0.03 m/s. Note that for this period the lower quartile is the lowest (-0.02 m/s) and the IQR encompass more negative values.

The post hoc test for the seasonal analysis showed winter and spring as the periods with the most significant statistical differences, followed by spring and autumn differences. The bimonthly analysis showed that the periods of May-June and September-October as those with the main differences, and the group of two months that belongs to the winter-spring periods present more of a transitory behaviour.

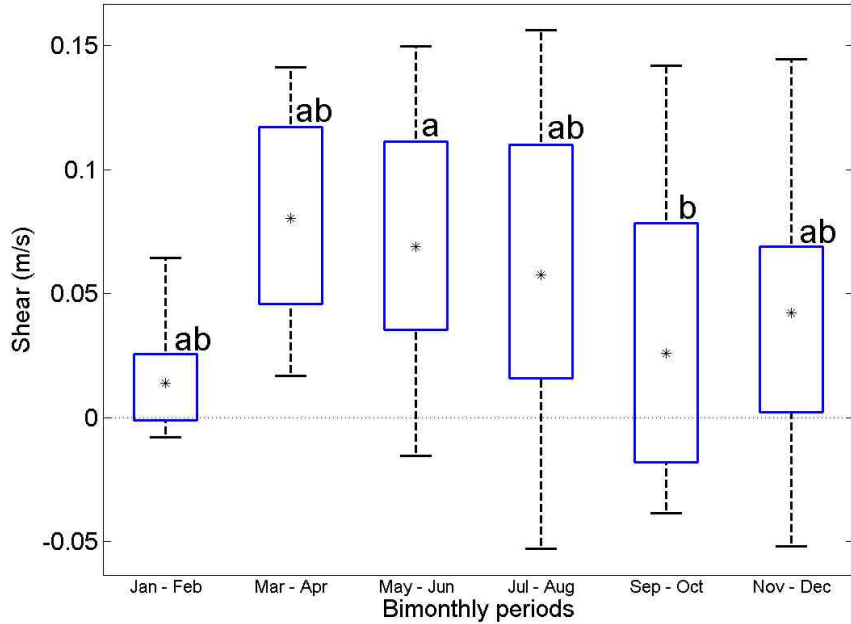


Figure 3.14 - Shear at zero crossing (m/s) bimonthly distribution. Mean represented by asterisks and letters indicates groups differences obtained after Kruskal-Wallis test ( $P > 0.05$ ) and Dunn post hoc comparisons.

In Figure 3.15 is possible to assess the weight of negative shear together with shear  $> 0.1$  m/s for each bimonthly period. In the January-February period, negative shear represents 40% of the cases and no shear  $> 0.1$  m/s is observed. March-April also present no negative shear but shear  $> 0.1$  m/s represents 29%. The period of May-June, in 5% of the cases shear is negative and 30% is  $> 0.1$  m/s. In July-August 18% of the cases, shear is positive and 27% is  $> 0.01$  m/s. In September-October, the percentage of negative shear reach 46%. Shear with values  $> 0.01$  m/s happens 17% of the time. For November-December, the positive-negative ratio is 79% and 21% respectively with 21% of shear  $> 0.1$  m/s.

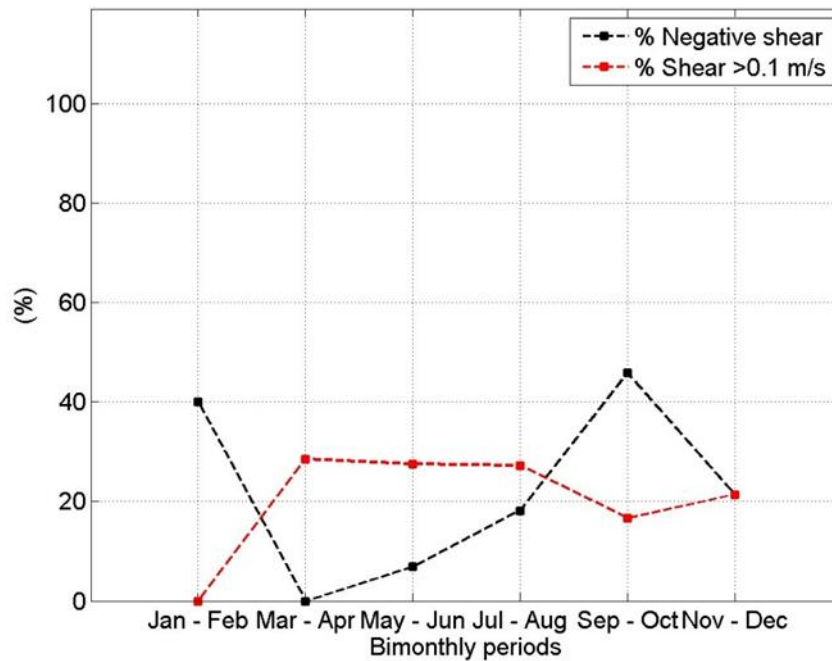


Figure 3.15 - Percentages of negative shear at inversion (black), together with percentage of shear >0.1 m/s (red) for each period of two months.

### 3.2.3.3 Summary of main observations

Shear at zero-crossing analysis indicates that the counter-currents tends to start near the bottom most of the times. Values of positive shear can reach 0.16 m/s which is an order of magnitude larger than the maximum negative shear -0.05 m/s.

Along the year the main differences on Shear values showed to be between the late spring time, against early autumn.

Interestingly shear values has a broad range from March until December, but the transition to January-February period is very abrupt. On average shear is weak and less variable during winter (preferably in January and February). Extreme values happen in the other seasons. The period of March until August has the most positive shear values while September and October is more likely to occur both situations and with a highest percentage of negative shear.

### 3.2.4 Slope at zero-crossing

Slope distribution (Figure 3.16) shows that near bed inversions occur with a much lower acceleration than near surface. Note that slope increase with negative values. Mean value and minimum near surface are approximately double of the near bed. Near surface present a mean value of  $-0.4 \times 10^{-5} \text{ m/s}^2$  with STD  $2.25 \times 10^{-6} \text{ m/s}^2$  and minimum of  $-1 \times 10^{-5} \text{ m/s}^2$ . Near bed mean value is  $-0.17 \times 10^{-5} \text{ m/s}^2$  with STD  $0.8 \times 10^{-6} \text{ m/s}^2$  and the minimum reach  $-0.4 \times 10^{-5} \text{ m/s}^2$ . For both layers when slope is less accentuated it is around  $0.2 \times 10^{-6} \text{ m/s}^2$ .

As described in the parameters definition Slope will be also assessed in terms of high and low slope. Near the surface, high slope (mean minus STD) is  $\leq -0.6 \times 10^{-5} \text{ m/s}^2$  and

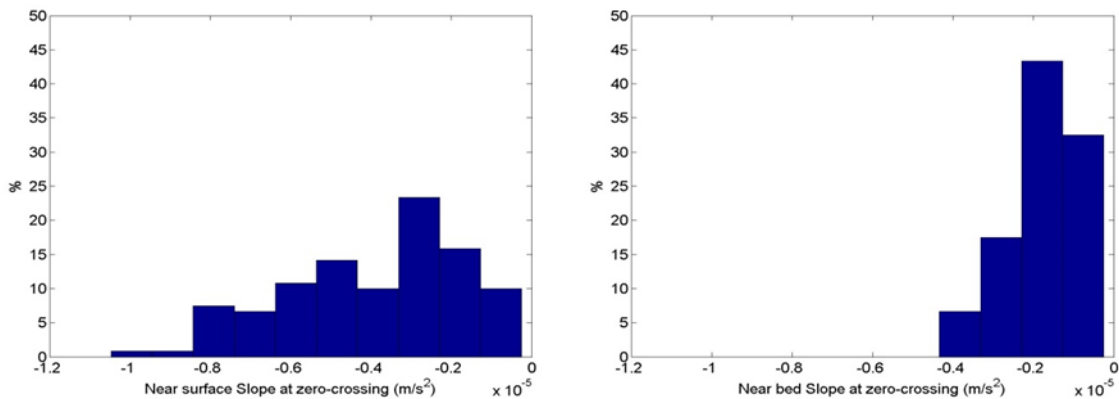


Figure 3.16 - Slope at zero-crossing all data distribution. Near the surface layer left and near the bed layer right. represents 18%. Low slope (mean plus STD) is  $\geq -0.17 \times 10^{-5} \text{ m/s}^2$  and represent 17%.

#### 3.2.4.1 Seasons

In the surface layer Slope values does not oscillate much along the year. Generally, both layer present similar trend, higher slope in winter-spring and lower slope in summer-autumn (Figure 3.17).

Kruskal-Wallis test showed significant statically differences ( $P > 0.05$ ) only for the near bed Slope at zero-crossing. The post hoc comparisons indicated that summer and autumn are distinct from winter and spring as being a transitory period.

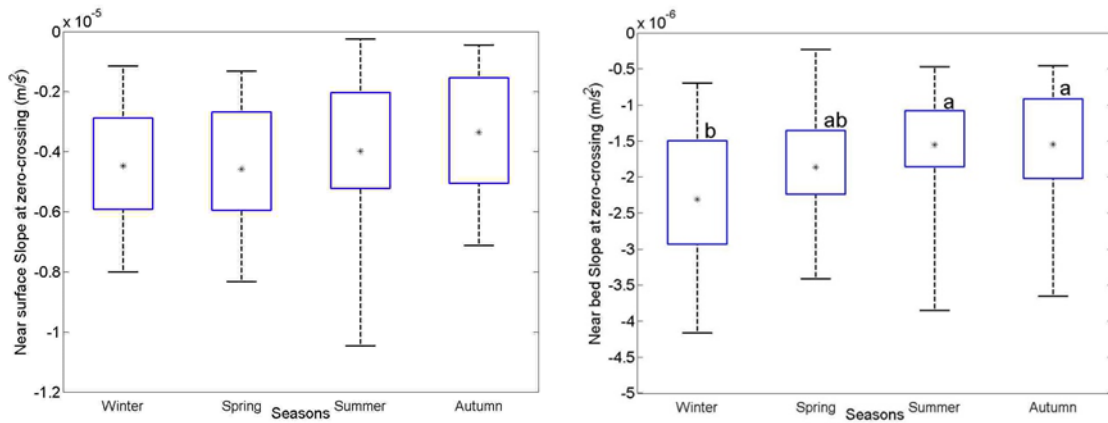


Figure 3.17 - Slope at zero-crossing ( $m/s^2$ ) seasonal distribution. Near surface left and near bed right. Mean represented by asterisks and letters indicates groups differences obtained after Kruskal-Wallis test ( $P > 0.05$ ) and Dunn post hoc comparisons.

Figure 3.18 confirm the tendency of decreasing slope towards autumn as the frequency of low slope increases from winter to autumn. Near the surface the frequency of high slope do not fluctuate along the year, while near the bed high slope has its maximum in winter 40% and minimum in autumn 10%.

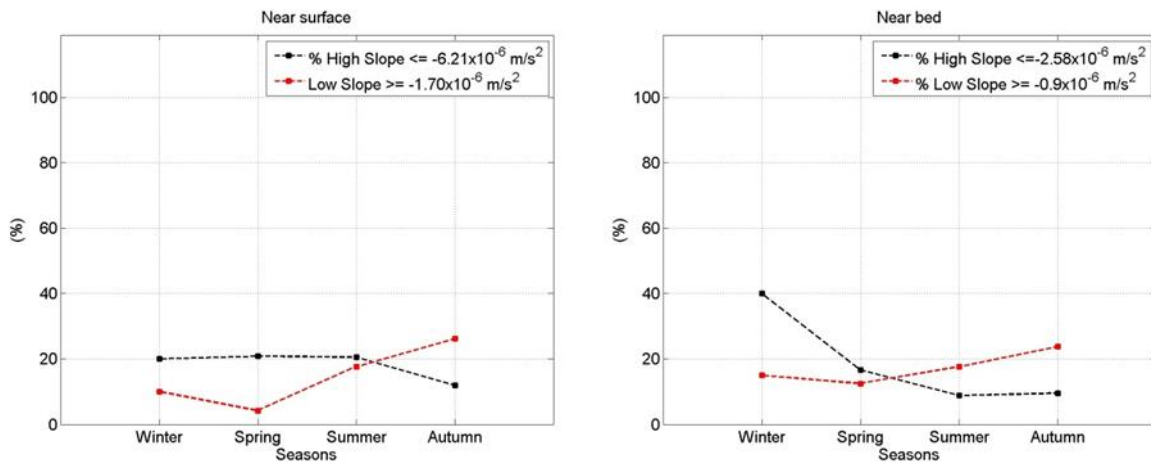


Figure 3.18- Seasonal percentages of High slope at zero-crossing in black and Low slope at zero crossing in red. Near the surface left and near the bed right.

### 3.2.4.2 Bimonthly scale analysis

When Slope at zero-crossing is plotted in function of two months period (Figure 3.19) the tendency of decreasing slope towards autumn disappear and fluctuations of the mean values are not marked. Again, the Kruskal-Wallis test showed significant statically

differences ( $P > 0.05$ ) only for the near bed Slope at zero-crossing. The periods flagged as different by the post hoc comparison was the period of September-October against November-December. Note that the period of September-October presents the lowest mean  $1.7 \times 10^{-6} \text{ m/s}^2$  and one of the lowest IQR  $6.6 \times 10^{-6} \text{ m/s}^2$  and November-October the Highest

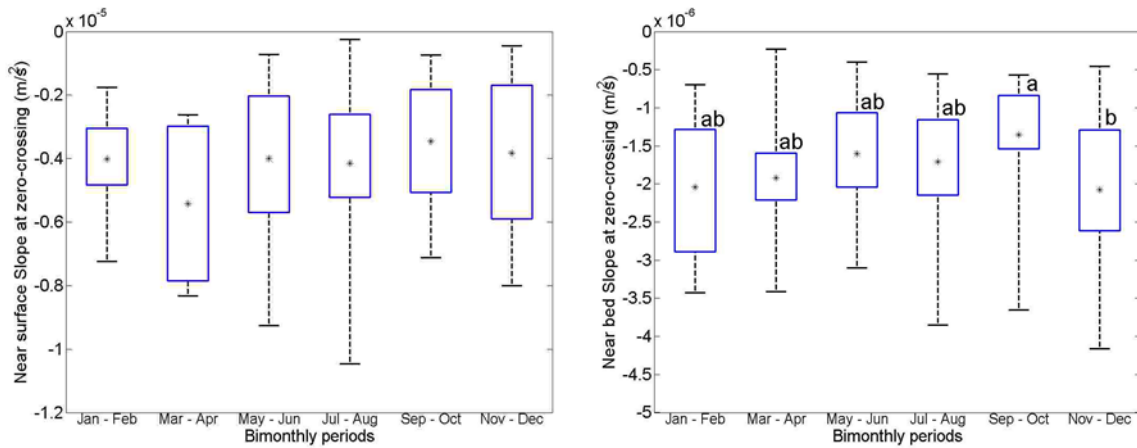


Figure 3.19 - Slope at zero-crossing ( $\text{m/s}^2$ ) bimonthly distribution. Near surface left and near bed right. Mean represented by asterisks and letters indicates groups differences obtained after Kruskal-Wallis test ( $P > 0.05$ ) and Dunn post hoc comparisons mean  $2 \times 10^{-6} \text{ m/s}^2$ .

The fluctuation of high slope near the bed is not so marked (Figure 3.20), but as in the seasonal analysis, during winter months is when high slopes are more present.

Near the surface, the percentage of low slope reach the maximum in the period from September until December (25%). Near the bed only the period of September-October presents a sharp increase on the low slope frequency that reaches 33%, 3 times more than the previous period July-August with 9%.

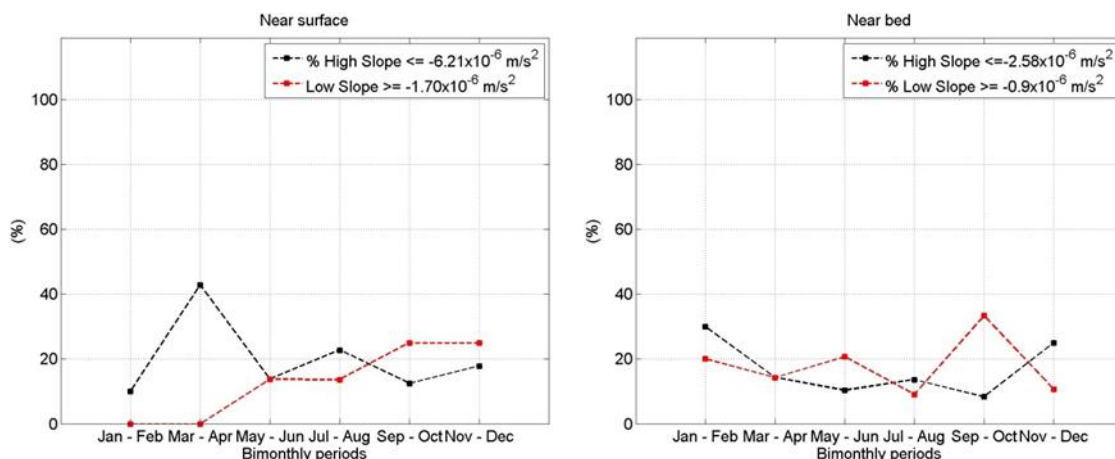


Figure 3.20 - Bimonthly percentages of High slope at zero-crossing in black and Low slope at zero crossing in red. Near the surface left and near the bed right.

### 3.2.4.3 Summary of main observations

Along the year, slope at zero-crossing does not present strong fluctuations near the surface.

Near the bed generally, winter Current inversion occur with a higher acceleration and in autumn the opposite. The increase on the percentage of low slope towards autumn is what suggests the deceleration on the current inversion. The period of September and October is where the most pronounced change is observed.

### 3.2.5 Slope Differences

Figure 3.21 represents the whole data distribution for Slope at zero-crossing differences (Slope near surface minus slope near bed). When slope differences are positive it means that near the bed layer had a more accentuated slope than near the surface. As described above, near bed slope is generally weaker than near surface, this way, Slope differences is majority negative occurring 90% of the time recorded. For the 10% of positive slope differences values are much lower than the opposite situation the mean of all positive values of slope differences is  $0.7 \times 10^{-6} \text{ m/s}^2$ .

The differences range between  $-8.3 \times 10^{-6} \text{ m/s}^2$  and  $1.9 \times 10^{-6} \text{ m/s}^2$ . The mean value is  $2.22 \times 10^{-6} \text{ m/s}^2$  (STD  $1.9 \times 10^{-6} \text{ m/s}^2$ ). As described in the parameters definition the Slope differences will be also assessed in terms of high negative slope differences (mean minus STD). For the whole data set it represent 16% of the cases.

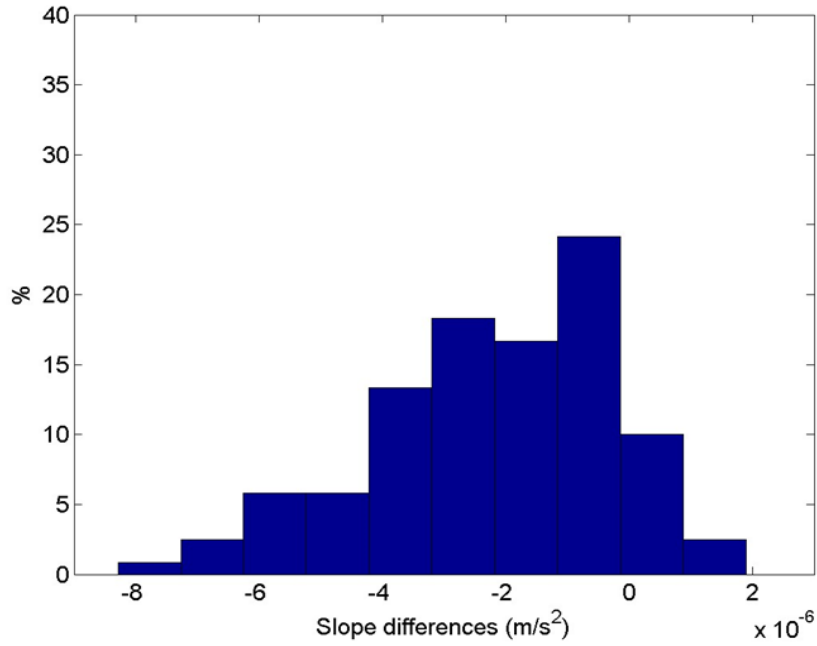


Figure 3.21- Slope differences (m/s<sup>2</sup>) all data distribution.

### 3.2.5.1 Seasons

Seasonal distribution of Slope differences in Figure 3.22 shows that in autumn is when the mean value is the closest to zero  $-1.80 \times 10^{-6} \text{ m/s}^2$  and STD  $1.95 \times 10^{-6} \text{ m/s}^2$  and both layers tend to invert with similar acceleration. In summer, the variability is increased. This

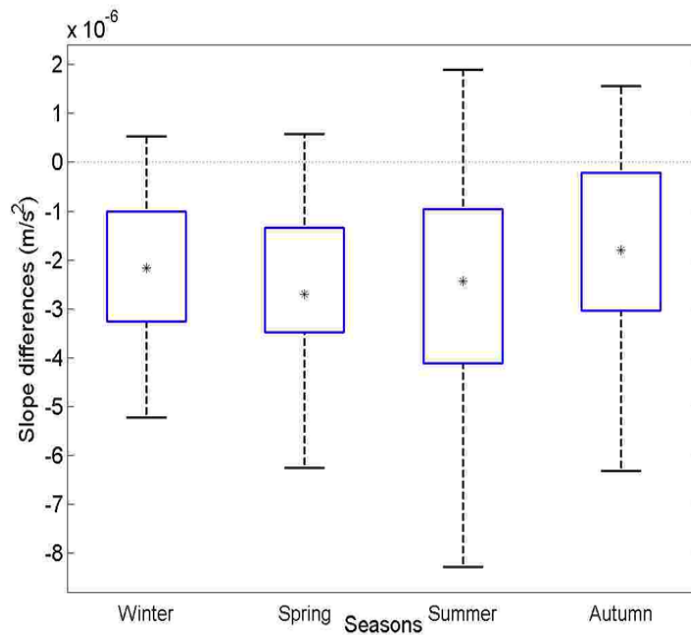


Figure 3.22 - Slope differences (m/s<sup>2</sup>) seasonal distribution. Mean

period presents the highest STD  $2.4 \times 10^{-6} \text{ m/s}^2$  and the highest IQR  $3.1 \times 10^{-6} \text{ m/s}^2$ .

The main feature in the seasonal distribution of Slope differences is that, in the summer period, values present a broader range. In fact, summer present both the highest percentages of positive slope differences (15%) and the highest percentage of high negative slope differences (21%). In the other hand winter period present the lowest percentages of both extreme values (Figure 3.23).

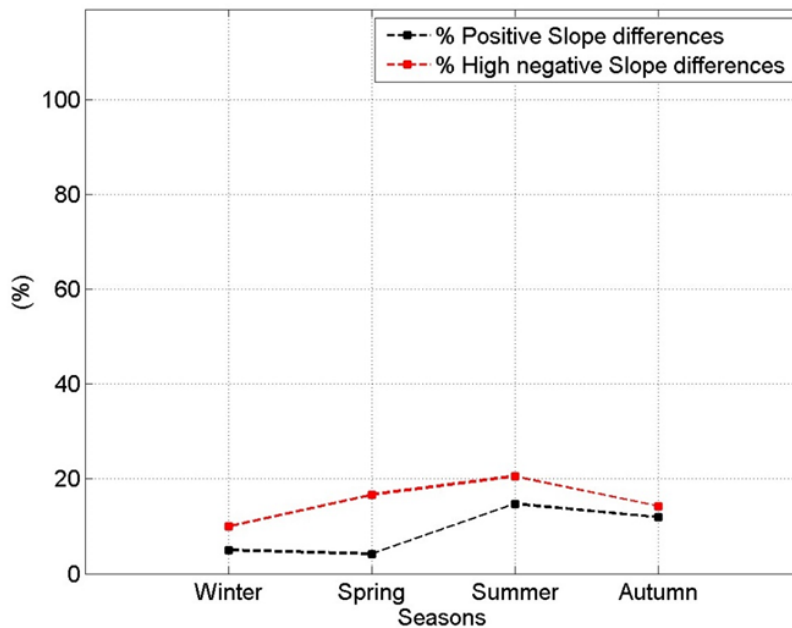


Figure 3.23 - Seasonal percentages of positive slope differences in black and high negative slope differences in red.

### 3.2.5.2 Bimonthly time scale analysis

When Slope differences distribution is plotted in the bimonthly time scale (Figure 3.24), it is observed that the mean values do not fluctuate significantly. Data variability for the period of January-February is the lowest. IQR is equal to  $6.6 \times 10^{-7} \text{ m/s}^2$ , one order of magnitude lower than the other periods.

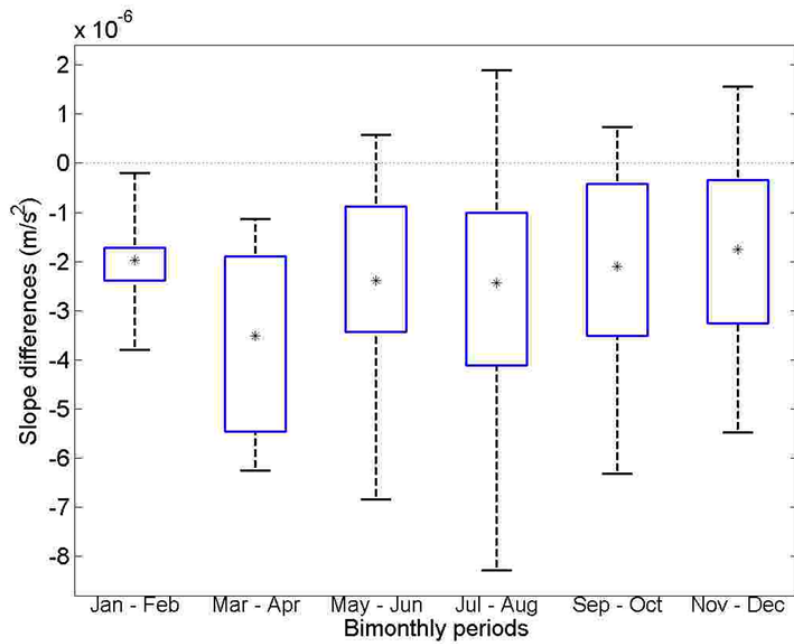


Figure 3.24 - Slope differences ( $m/s^2$ ) bimonthly distribution.

Figure 3.25 shows that high negative slope differences may happen all year but not in January-February. There is a peak on the percentage of high negative slope differences for the period of March-April.

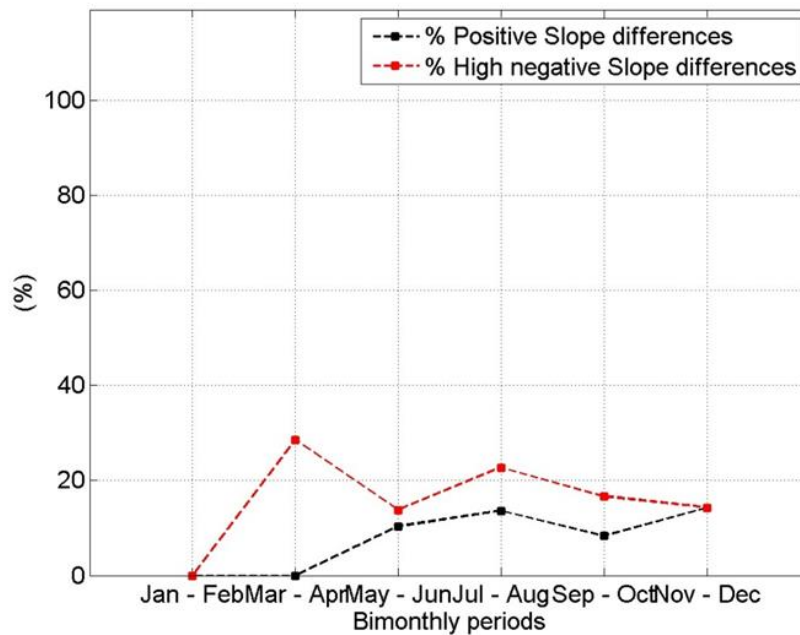


Figure 3.25 - Bimonthly percentages of positive slope differences in black and high negative slope differences in red.

Positive Slope differences also follows the same trend, it appears with low frequency (maximum 14% for the period of November and December) from May until December.

### 3.2.5.3 Summary of main observations

During the first two months of the year, both layers invert with minimum slope differences. For the time recorded, near surface had always a higher acceleration with only 12 events where near bed had higher acceleration and when it happened the difference was very low.

### 3.3 Parameters integrative analysis

To first assess the relationship between parameters, scatter plots were created, and no strong correlation was found in most of the cases. In Figure 3.26 where Shear at zero-crossing is plotted against Slope at zero-crossing there is an indication of inverse correlation for the surface layer during spring (Figure 3.26 left). The same pattern is not observed near the bed as the slope is a parameter with very low fluctuations for this layer.

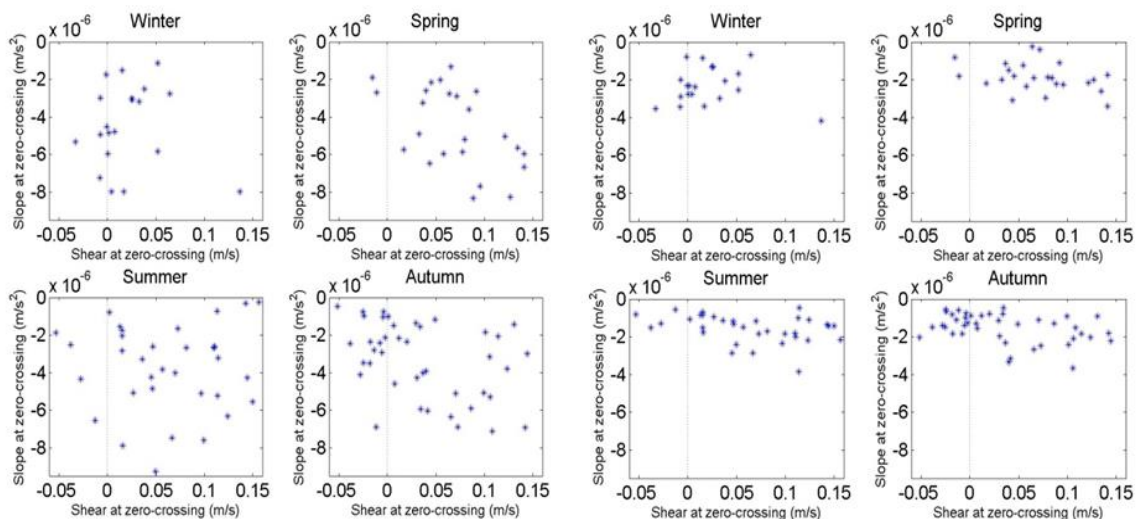


Figure 3.26 - Seasonal Scatter plot of Shear at zero-crossing versus Slope at zero-crossing. Near the surface left and near the bed right.

In Figure 3.27 the scatter of Shear at zero-crossing versus peak delay highlight and summarize the types of inversion that can occur.

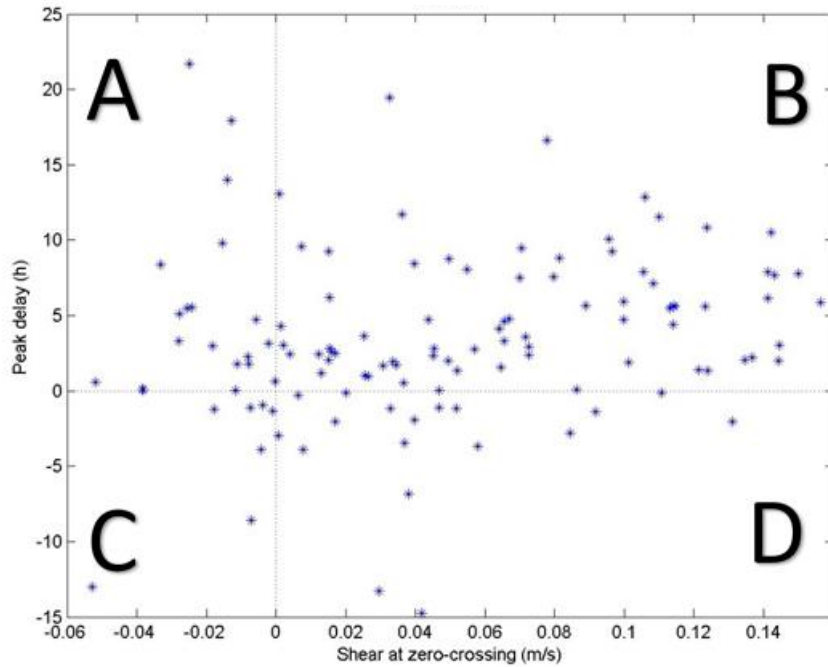


Figure 3.27 - Shear at zero-crossing versus peak delay all data. Black letters highlight the inversion types proposed here

Type A – occurs 16.7% of the observed time. CCC Type A, starts to turn near the bed and when the average layer crosses zero, near surface had already changed sign while near bed is still equatorward (Figure 3.28).

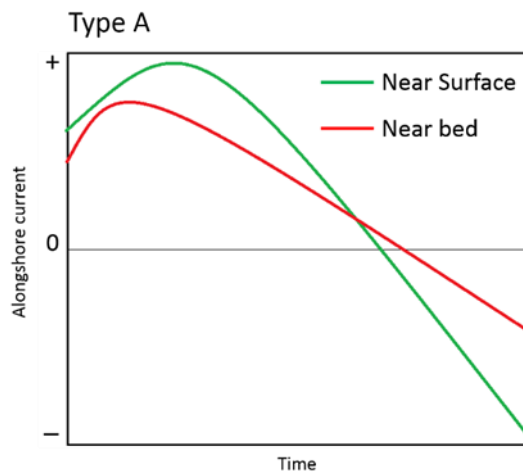


Figure 3.28 - Scheme for current inversion Type A, where peak delay is positive and shear at zero-crossing is negative

Type B – is the most common type (62.5%). CCC Type B, starts to turn near the bed and when the average layer crosses zero, near bed had changed sign and near surface is still

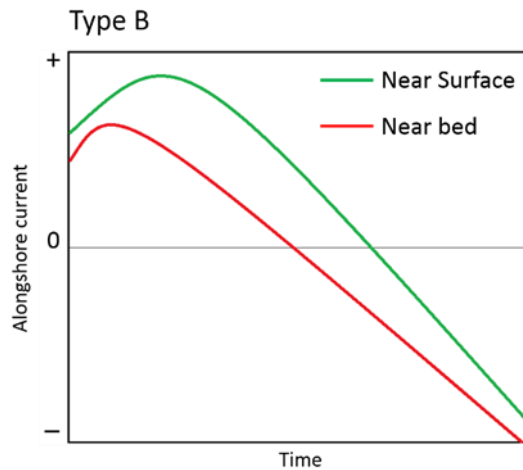


Figure 3.29 - Scheme for current inversion Type B, where peak delay is positive and shear at zero-crossing is positive. equatorward (Figure 3.29).

Type C – is a rare case and occurs only 5.8% of the time. Inversions Type C starts to turn near the surface and when the average layer crosses zero, near surface had already changed sign while near bed is still equatorward (Figure 3.30).

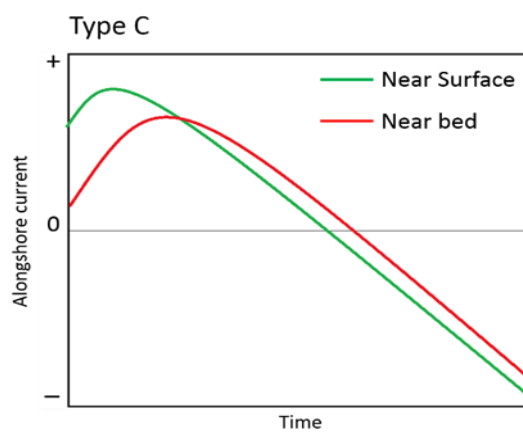


Figure 3.30 - Scheme for current inversion Type C, where peak delay is negative and shear at zero-crossing is negative

Type D – Inversions type D starts to turn near the surface and when the average layer crosses zero, near bed had changed sign and near surface is still equatorward. It happens 15% of the time (Figure 3.31).

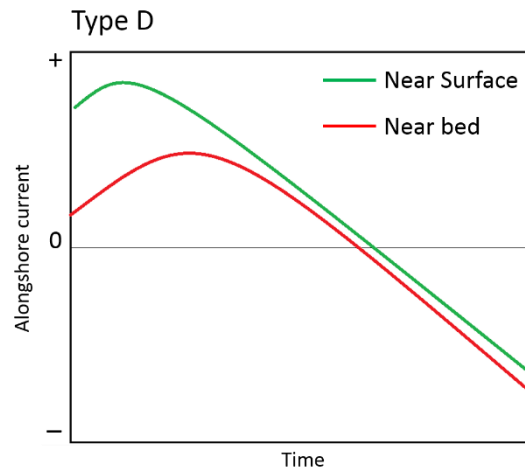


Figure 3.31 - Scheme for current inversion Type D, where peak delay is negative and shear at zero-crossing is positive.

When these 4 different types of inversions are plot seasonally (Figure 3.32) it gains more shape and it is possible to track when a specific type occurs more preferably.

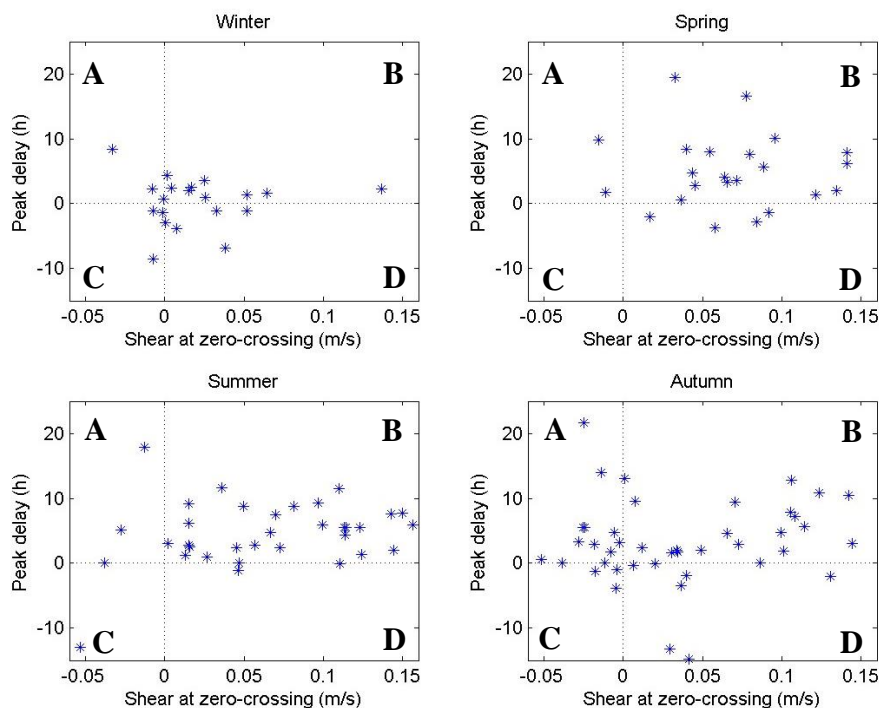


Figure 3.32 - Seasonal scatter plot of shear at zero-crossing versus peak delay.

In winter inversions are less variable, all 4 inversions types may occur but, they tend to zero on both parameters. During this season both layers act well coupled as CCCs develops.

In spring and summer, CCCs type B occurs with more predominance (75% and 80% respectively). Contrary to winter, spring do not present many inversions where values of both parameters tend to zero.

In autumn is the time of the year where CCCs type A becomes more active occurring 28% of the time.

#### **4. Discussion**

Poleward coastal counter-currents (CCCs), are recurrent features of the Eastern Boundary Upwelling Systems of the world that normally oppose the equatorward flow of upwelling origin. Typically, CCCs advect warm water after upwelling events and temporarily displacing the previously upwelled colder water offshore (Melton *et al.*, 2009; Relvas and Barton, 2002; Send *et al.*, 1987). These currents can alter the water quality, either by the depletion of nutrients (G. Navarro *et al.*, 2006; Rosa, 2016) or by the transport of pollutants.

They have been described in several regions such as Peru-Chile (Strub, *et al.*, 1995) in the South African Benguela Current upwelling system (Fawcett *et al.*, 2008), and in the California Current upwelling system (Dever *et al.*, 2004; Kosro, 2005; Largier *et al.*, 1993; Lentz and Chapman, 1989; Melton *et al.*, 2009; Send *et al.*, 1987; Washburn *et al.*, 2011; Winant *et al.*, 1987; Woodson *et al.*, 2009)

In Santa Barbara Channel (SBC) in California, where the coastline orientation is similar to the western coast of the Iberian Peninsula; Melton *et al.* 2009, through *in situ* current and temperature measurements, described the poleward flow as seasonal feature in the upwelling season, generated in response of adjustment of the unbalanced alongshore pressure gradient (APG) and wind relaxation.

Relvas and Barton (2002) also suggest APG as the main driver of CCCs in the GC, but Garel *et al.* (2016) had shown that poleward flow occur  $\approx 42\%$  of the time, with no significant variations between summer and winter. Even though wind relaxation theory is

reasonable to explain CCCs during the upwelling season in the GC, it fails to explain the occurrence of CCCs in other seasons.

García-Lafuente *et al.* (2006) also proposed that in summer waters in the easternmost part of the Gulf can be rapidly heated in shallow areas and thus contribute to surface tilt by vertical thermal expansion. However, the lack of seasonality in CCCs patterns (i.e., without predominance of CCCs events during the upwelling season) challenge the hypothesis and rather suggest that CCCs result from various complex processes that may combine or act in isolation.

The forces involved in the process that develop CCCs in the GC are poorly understood as studies performed in the region are mainly based on short time-series (García-Lafuente *et al.*, 2006; Lobo *et al.*, 2004; Sánchez *et al.*, 2006) or remotely sensed temperature images (Fiúza, 1983; Fiúza, *et al.*, 1982; Folkard, Davies, Fiúza *et al.*, 1997; Sanchez and Relvas, 2003; Stevenson, 1977; Vargas *et al.*, 2003). Criado-Aldeanueva *et al.* (2009) performed the most extensive analysis on a multi-year (2002, 2004, 2005) current time-series and analysed the seasonal and interannual variability of the surface circulation, but so far, no conclusive arguments evidenced the main driving forces of the CCCs in the GC.

The results of the present study showed for the first time a composite of parameters describing the vertical structure and timing of CCCs focused at beginning of the flow. Therefore, the aim of this study was to address potential responsible forces for the development of these type of current based on types of inversion defined here.

In general, CCCs starts to develop near the bottom. The studied time-series shows that 77% of the times the bottom layer changes direction before the surface. This could be explained by the difference in momentum between near surface and near bed. Results also showed that near the surface, water moves most of the times faster than the bed layers (due to bottom stress), and requires therefore more energy to decelerate and change direction than the bed layer. Even though near the bed presented slower velocity, Peak delay analysis showed that, 79% of the inversion registered, the flow is still accelerating equatorward in the surface layer while in the bottom, it has started to decelerate and invert in the poleward direction. It seems that the surface layer is still being affected by a force that is no longer affecting the bed, or they are being affected by different forces in the opposite directions.

Garel *et al.* (2016) also identified a two-layer flow during start of CCCs (see negative PC2 peaks in their Figure 11-d). At the start of all CCCs events analysed by the author, 62%

of the time near bed becomes poleward first. Although the results presented here and Garel *et al.* (2016) study share almost the same data set (this study contains a longer period of observation), no quantification or seasonal distinction of shear was made before.

According to Rossby (1938) a wind origin APG, can trigger a counter-flow near the bottom if we have a double-layer (stratified) ocean. The surface slope generated by the wind would have an opposite orientation in the interface of the two layers. The adjustment of this gradients would generate a counter-flow near the bottom. Rossby's theory is dedicated to deeper regions of the ocean and may not be applicable in the GC of Cadiz but in summer stratification is enhanced and the shelf extension is short in some parts of the CG that may allow such mechanism to take place. Notice that the shelf is particularly narrow off Armona, where the analysed ADCP records were obtained.

The time current takes to invert completely (from a peak of maximum acceleration in the equatorward direction to the next peak in the poleward direction) is on average 2 days. This would take place one day before and the first day out of a 3-day (on average) duration event as described by Garel *et al.* (2016).

Slope at zero-crossing analysis showed that near the surface present a higher acceleration. During the time recorded, only in 12 events near bed had higher acceleration, and when it happened the difference was very small.

In summary, the general CCCs set up is defined by deceleration in the equatorward direction, and direction change near the bed first. The near surface layer is faster and present a higher acceleration during inversions. The duration of an inversion is generally the same in

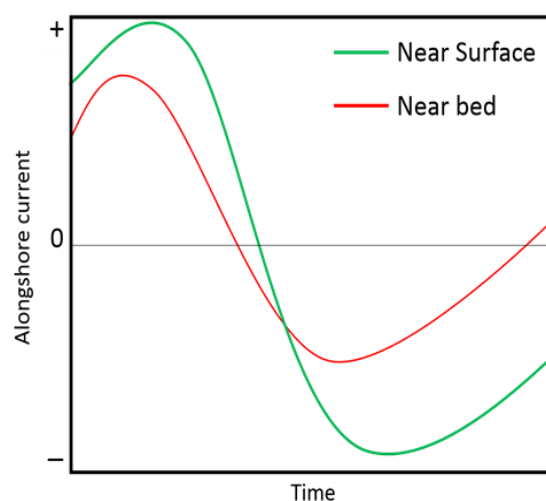


Figure 4.1 - General model of CCCs inversions. Near the bed (red) decelerates and changes direction first. Near the surface present higher acceleration (slope) and inversion duration is very similar in both layers.

both layers. Figure 4.1 exemplifies this general model of Inversions described above.

Note that the model represented in the figure is the Type B proposed in the parameters integrative analysis section (Figure 3.29). The main difference is that the general model integrates more parameters. In fact, Type B is the type that occurs most frequently (62.5%), but from the 3 other types created by the conjugation of peak delay and shear at zero-crossing, 2 occur with significant frequency (Type A and D with 16.7% and 15% respectively). Type A, differs from the general model by the presence of negative shear at zero-crossing while peak delay is positive like in the model. Type D represents the opposite of the general model, negative peak delay and positive shear.

Type C is not considered an important type, first because it has a very low occurrence in the total data set, and secondly, because most of the inversions registered that

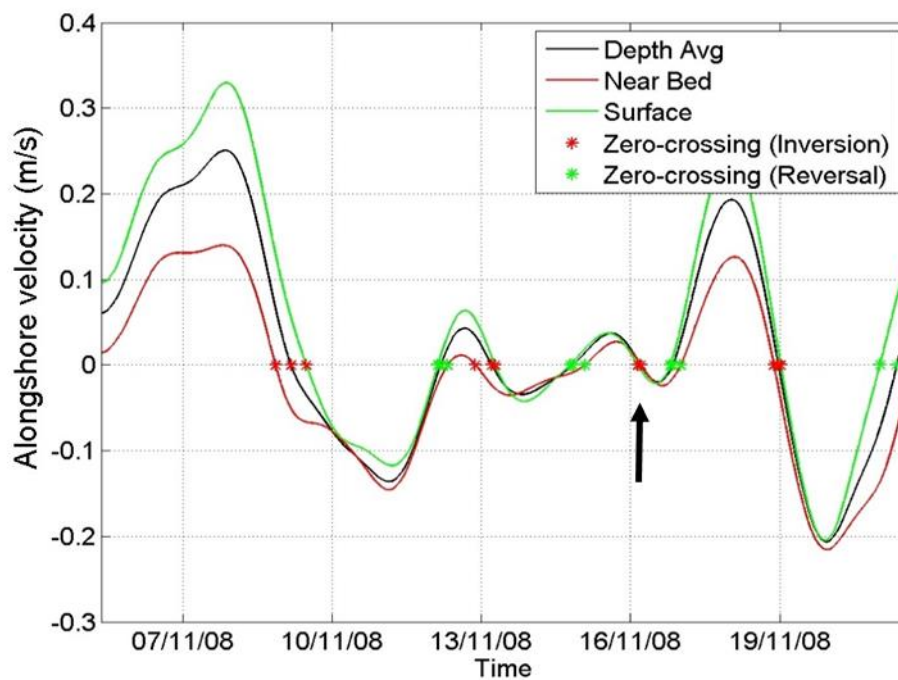


Figure 4.2 - Three-layer vertical velocity (m/s) profile. Depth average velocities (black line), Near bed (red line) and near the surface (green line). Black arrow indicates the event of 16/11/2008 to exemplify an inversion Type C.

falls into inversion Type C, were inversion of weak flows. Some of those inversions also occurred after previous oscillations and other Inversion/reversal of higher magnitude as shown in Figure 4.2 for the event of 16/11/2008.

Interestingly, the inversion exemplified on the Figure 4.2 share similarities with the example of Melton *et al.* (2009) in their figures 6 and 7, where after an event of favourable

upwelling winds, relaxation gives rise to a strong poleward flow followed by several noisy oscillations.

Type D, was also not considered, although it represents 15% of the whole data set. Its distribution along seasons did not prove to be significant. It reaches its highest percentages in winter (25%), but most of these inversions values of shear or peak delay are close to zero and therefore does not show a well-defined pattern.

## **4.1 Seasonal variability**

Some of the actual theories for the development of the CCCs in the GC, suggest forces that present a seasonal frequency. (Criado-Aldeanueva *et al.*, 2009; García-Lafuente *et al.*, 2006; Mauritzen *et al.*, 2001; Relvas and Barton, 2002)

Although Garel *et al.* (2016) show no seasonality on the occurrence of CCCs, the main results of parameters seasonally analysed, showed statistically significant differences (Kruskall-Wallis  $P < 0,05$  and the post hoc comparisons) among seasons and some bimonthly periods.

### **4.1.1 Winter**

The results of peak delay, shear at zero-crossing and near bed slope at zero-crossing (Figures 3.2, 3.12, 3.17 respectively) are consistent with the existence of two distinct patterns of inversions between winter and spring-summer. Winter is marked by a barotropic flow where values of peak delay and shear at zero-crossing tend to zero. Note that near the surface, the slope is almost constant along the year and, is always higher than near the bed. It is in winter that near the bed slope values are more accentuated and becomes closer to surface values. This winter homogenization of the water column compared to summer was also referred by Garel *et al.* (2016) with temperature records and hypothesized by Criado-Aldeanueva *et al.*, (2009).

In accordance with the features observed in winter inversions, another type is suggested here, hereafter called type 0: a more homogeneous vertical structure during inversions.

In winter, the atmospheric set up of the AH favour the poleward alongshore wind component to become more frequent (Chase, 1956). Winds also becomes stronger (Garel *et al.*, 2016) being able to act more efficiently over the whole water column. In addition, upwelling associated APG is expected to be less effective since favourable winds becomes less frequent.

The baroclinic characteristic of type 0 reflects the expected effect of the possible winter forces where wind must play a more important role. In fact, Criado-Aldeanueva *et al.* (2009) proposed that winter homogenization of the water column, together with favourable winds and the presence the entrainment of Atlantic waters entering the SG from south would (as proposed by Mauritzen *et al.* [2001]) generate poleward flows without strong external forcing.

#### **4.1.2 Spring-summer**

The spring-summer Inversions characteristics are marked by the increase of baroclinicity and predominance of Type B. During this period, near bed starts to decelerate and, change direction before near the surface. Inversion Type B occurs 75% in spring and 82% in summer. If during this period forces are acting differently over layers, what forces could explain the pattern observed in type B?

Spring-summer is the upwelling season for the nearby Portuguese west coast region. In the southern coast, upwelling favourable winds (westerlies) also becomes more frequent but less effective than in the west coast (Relvas and Barton, 2002). The lack of correlation between tide gauge data and local winds suggests that winds are not responsible to generate APG in the region of GC (Sánchez *et al.*, 2006). APG is believed to be generated, in the south coast, by the frequent presence of the upwelling jets turning around the CSV and also due to sheltering effect of the coast orientation and local topography features that protected the south coast from the main upwelling favourable winds. This results in two distinct zones and pressure gradient between them (Relvas and Barton, 2005).

In the presence of the APG acting in the poleward direction, the whole water column would be susceptible to this force, and its effects would not depend on depth. The main alongshore wind direction opposes the APG and acts more efficiently over the surface layers. In this sense, the bottom layers would be under a mild effect of the wind and the associated bottom stress. When APG is strong enough it will break the force acting equatorward easier in the bottom layer while the surface is still under winds influence.

It has been reported that CCCs may occur without favourable winds (Garel *et al.*, 2016), excluding the possibility as the main driver. Therefore, a similar approach of the peak delay but including wind data, could be introduced in order to investigate if there is a lag between the near bed and the wind. A situation where near bed starts to decelerate in the equatorward direction before the surface and the wind is still accelerating (in the equatorward direction) would agree with the argument that layers are being affected by different forces (or same forces disproportionately).

Further approaches to study CCCs, could include analytical solutions in order to assess the possibility of this mechanism to be valid as in the generation of a poleward flow near the bed first, and also the mechanism proposed by Rossby (1938).

### **4.1.3 Autumn**

Autumn was characterized by the highest frequency of negative shear (Type A), but in general it was a transition period. The higher frequency of Type A in autumn brings more insights about the poleward wind influence on the CCCs development. This type is most frequent in a season where upwelling winds are less frequent and Levante (local poleward winds) winds becomes stronger (Criado-Aldeanueva *et al.*, 2009; Garel *et al.*, 2016). In type A near the surface changes sign before the bed which suggest the wind influence, but the fact that near the bed decelerates first, contradicts the possibility of the wind to be the trigger of the Inversions. Type A is in agreement with the mechanism proposed by Relvas and Barton (2002) that CCCs are APG driven but the effects can be augmented or diminished by wind forcing.

For the near bed slope at-zero crossing was found that winter and autumn presented statistically significant differences. The difference was marked by lower slope in autumn and

higher slope in winter. When analysed bimonthly, the difference is then more accentuated between September-October and November-December periods, with September-October period presenting low acceleration during inversions. September-October period also show a distinct pattern in the shear at zero-crossing bimonthly distribution, a higher frequency of event with negative shear shifts the mean value down. According to the mechanism proposed here, this could be a result of a diminishing APG or intensification of Levante winds.

Future characterization of the local wind could be used in order to verify if September-October present more of a transitory or a very well-defined wind distribution.

## **5. Conclusions**

Poleward flows in the GC are recurrent phenomenon and its occurrence had been reported all year around. The forces involved in the process that develop such flow in the GC are poorly known. This study, for the first time, performed an assessment focused on the CCCs set up with the objective to address possible driving forces based on defining different types of inversions.

Results showed that, although CCCs do not follow seasonality, there is a seasonal pattern in its set up. In winter inversions are more defined with near surface and near bed layers acting similarly. In spring-summer layers can be more detached and inversions occur with more variable patterns. The difference on these patterns gives rise to the hypothesis of existence of several drivers that may act separately or together.

Based on the setup patterns, 3 main types of current inversions were defined, and they are well distributed along seasons:

Type 0 – Winter, homogeneous profile.

Type B – Spring-summer, baroclinic with near bed layer changing direction first.

Type A – Autumn, wind influence with higher occurrence of near the surface changing direction first.

Type 0 reflects the effect of strong winds and storms,

Types B and A bring insights that APG is the mechanism responsible for CCCs development for most of the year. A mechanism is proposed to explain the main features of the two types: flow starts to decelerate (in the equatorward direction) first near the bed.

The mechanism is defined by the presence of APG force acting over all layer in the poleward direction, but the equatorward winds still holds the surface layers. The result is that the bottom layers become more susceptible to be dominated by APG force.

This mechanism could be tested in a future work considering real wind data together with sea level anomalies (satellite or pressure gauges). The same approach used for this study could be used: define some parameters and try to match up the 3 variables information. Furthermore, the analytical solution of the momentum equation would be fundamental to quantify and point out which is/are the main driving forces of CCCs.

## 6. References

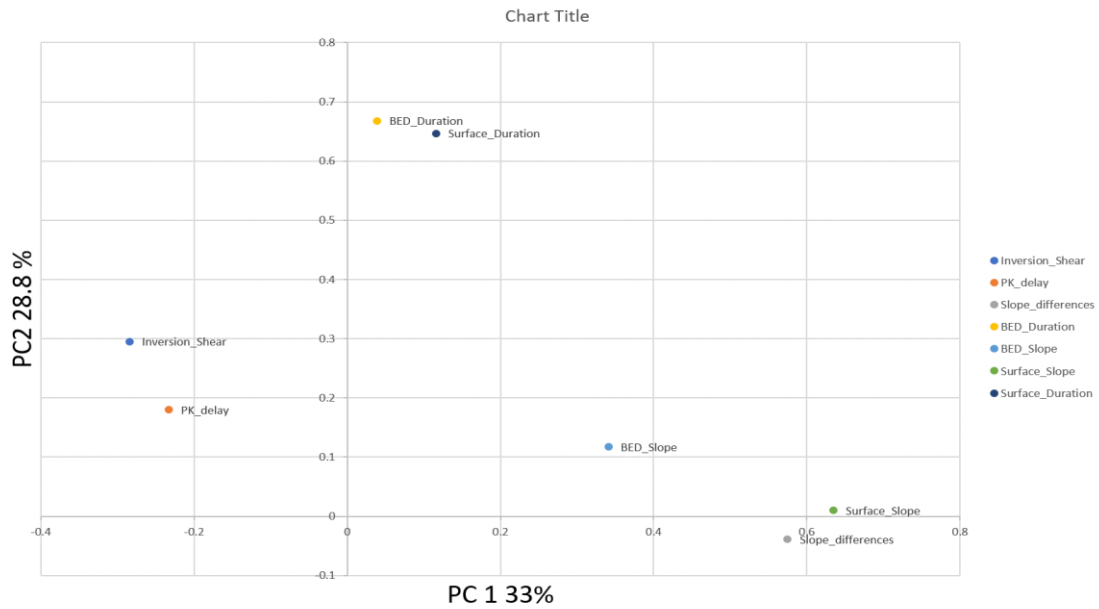
- Criado-Aldeanueva, F., Garcia-Lafuente, J., Navarro, G., & Ruiz, J. (2009). Seasonal and interannual variability of the surface circulation in the eastern Gulf of Cadiz (SW Iberia). *Journal of Geophysical Research: Oceans*, *114*(1), 1–11. <https://doi.org/10.1029/2008JC005069>
- García-Lafuente, J., Delgado, J., Criado-Aldeanueva, F., Bruno, M., del Río, J., & Miguel Vargas, J. (2006). Water mass circulation on the continental shelf of the Gulf of Cádiz. *Deep-Sea Research Part II: Topical Studies in Oceanography*, *53*(11–13), 1182–1197. <https://doi.org/10.1016/j.dsr2.2006.04.011>
- García, C. M., Prieto, L., Vargas, M., Echevarría, F., García-Lafuente, J., Ruiz, J., & Rubin, J. P. (2002). Hydrodynamics and the spatial distribution of plankton and TEP in the Gulf of Cadiz (SW Iberian Peninsula). *Journal of Plankton Research*, *24*(January), 817–833. <https://doi.org/10.1093/plankt/24.8.817>
- Garel, E., Laiz, I., Drago, T., & Relvas, P. (2016). Characterisation of coastal counter-currents on the inner shelf of the Gulf of Cadiz. *Journal of Marine Systems*, *155*, 19–34. <https://doi.org/10.1016/j.jmarsys.2015.11.001>
- Harms, S., & Winant, C. D. (1998). Characteristic patterns of the circulation in the Santa Barbara Channel. *Journal of Geophysical Research*, *103*, 3041–3065.

- Mauritzen, C., Morel, Y., & Paillet, J. (2001). On the influence of Mediterranean Water on the Central Waters of the North Atlantic Ocean. *Deep-Sea Research I*, 48, 347–381. [https://doi.org/10.1016/S0967-0637\(00\)00043-1](https://doi.org/10.1016/S0967-0637(00)00043-1)
- Mazé, J. P., Arhan, M., & Mercier, H. (1997). Volume budget of the eastern boundary layer off the Iberian Peninsula. *Deep-Sea Research Part I: Oceanographic Research Papers*, 44(9–10), 1543–1574. [https://doi.org/10.1016/S0967-0637\(97\)00038-1](https://doi.org/10.1016/S0967-0637(97)00038-1)
- Melton, C., Washburn, L., & Gotschalk, C. (2009). Wind relaxations and poleward flow events in a coastal upwelling system on the central California coast. *Journal of Geophysical Research: Oceans*, 114(11), 1–18. <https://doi.org/10.1029/2009JC005397>
- Navarro, G., & Ruiz, J. (2006). Spatial and temporal variability of phytoplankton in the Gulf of Cádiz through remote sensing images. *Deep-Sea Research Part II: Topical Studies in Oceanography*, 53(11–13), 1241–1260. <https://doi.org/10.1016/j.dsr2.2006.04.014>
- Navarro, G., Ruiz, J., Huertas, I. E., García, C. M., Criado-Aldeanueva, F., & Echevarría, F. (2006). Basin-scale structures governing the position of the deep fluorescence maximum in the Gulf of Cádiz. *Deep-Sea Research Part II: Topical Studies in Oceanography*, 53(11–13), 1261–1281. <https://doi.org/10.1016/j.dsr2.2006.04.013>
- Peliz, A., Dubert, J., Marchesiello, P., & Teles-Machado, A. (2007). Surface circulation in the Gulf of Cadiz: Model and mean flow structure. *Journal of Geophysical Research*, 112(C11), 1–20. <https://doi.org/10.1029/2007JC004159>
- Peliz, A., Marchesiello, P., Santos, A. M. P., Dubert, J., Teles-Machado, A., Marta-Almeida, M., & Le Cann, B. (2009). Surface circulation in the Gulf of Cadiz: 2. Inflow-outflow coupling and the Gulf of Cadiz slope current. *Journal of Geophysical Research: Oceans*, 114(3), 1–16. <https://doi.org/10.1029/2008JC004771>
- Relvas, P., & Barton, E. D. (2002). Mesoscale patterns in the Cape São Vicente (Iberian Peninsula) upwelling region. *Journal of Geophysical Research*, 107(C10), 1–23. <https://doi.org/10.1029/2000JC000456>
- Relvas, P., & Barton, E. D. (2005). A separated jet and coastal counterflow during upwelling relaxation off Cape S??o Vicente (Iberian Peninsula). *Continental Shelf Research*, 25(1), 29–49. <https://doi.org/10.1016/j.csr.2004.09.006>
- Rosa, A. I. M. (2016). *Estudo da variabilidade intra e inter-anual das trocas entre a Ria Formosa e o oceano - estudo de caso , a barra de Faro-Olhão.*
- Sanchez, R., & Relvas, P. (2003). Spring–summer climatological circulation in the upper layer in the region of Cape St. Vincent, Southwest Portugal. *ICES Journal of Marine Science: Journal Du ...*, 3139(3), 1352–1360. <https://doi.org/10.1016/S1054>

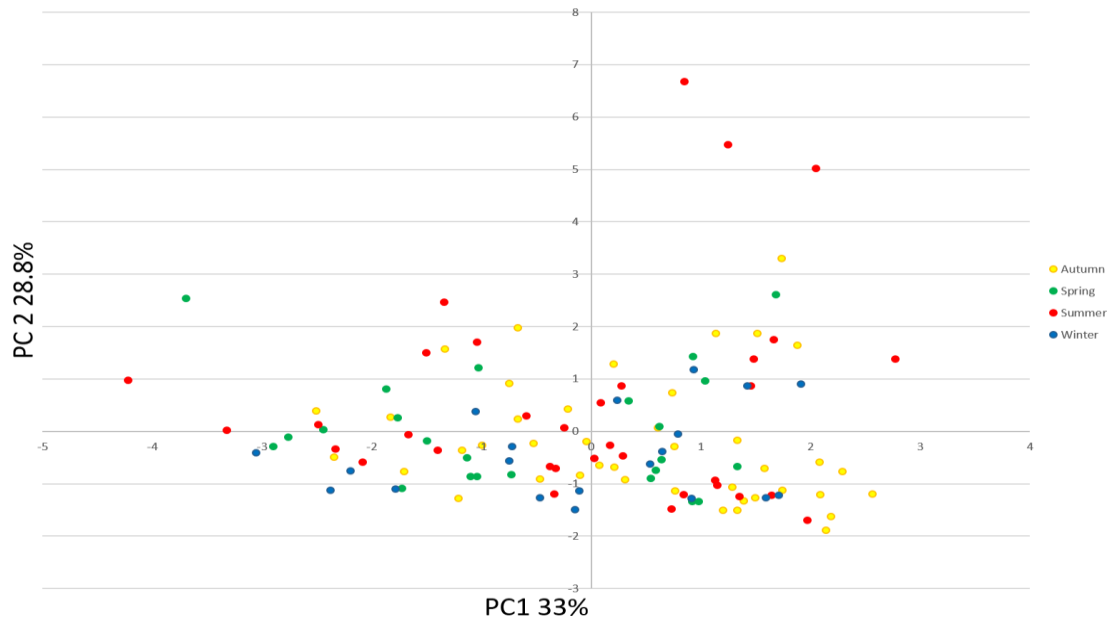
- Vargas, J. M., Garca-Lafuente, J., Delgado, J., & Criado, F. (2003). Seasonal and wind-induced variability of Sea Surface Temperature patterns in the Gulf of Cadiz. *Journal of Marine Systems*, 38(3), 205–219. [https://doi.org/10.1016/S0924-7963\(02\)00240-3](https://doi.org/10.1016/S0924-7963(02)00240-3)
- Washburn, L., Fewings, M. R., Melton, C., & Gotschalk, C. (2011). The propagating response of coastal circulation due to wind relaxations along the central California coast. *Journal of Geophysical Research: Oceans*, 116(12), 1–16. <https://doi.org/10.1029/2011JC007502>

## 7. Annex

### 7.1 Annex A – PCA results



Annex A.1- PCA applied to all parameters. Parameters loadings on the 2 maximum variance components.



Annex A.2 PCA applied to all parameters. Scores divided in seasons.